



PCCP

Morphological design strategies to tailor out-of-plane charge transport in conjugated polymer systems for device applications

Journal:	<i>Physical Chemistry Chemical Physics</i>
Manuscript ID	CP-PER-06-2021-002476.R1
Article Type:	Perspective
Date Submitted by the Author:	26-Jul-2021
Complete List of Authors:	Wenderott, Jill; University of Michigan, Materials Science and Engineering; Northwestern University, Materials Science and Engineering Dong, Ban; University of Michigan, Materials Science and Engineering Green, Peter; University of Michigan, Materials Science and Engineering; National Renewable Energy Laboratory

SCHOLARONE™
Manuscripts

Morphological design strategies to tailor out-of-plane charge transport in conjugated polymer systems for device applications

J. K. Wenderott^{1,2,‡}, Ban Xuan Dong^{1,‡}, and Peter F. Green^{1,3,*}

Received,
Accepted

DOI: 10.1039/x0xx00000x

The transport of charge carriers throughout an active conjugated polymer (CP) host, characterized by a heterogeneous morphology of locally varying degrees of order and disorder, profoundly influences the performance of CP based electronic devices, including diodes, photovoltaics, sensors, and supercapacitors. Out-of-plane charge carrier mobilities ($\mu_{\text{out-of-plane}}$) across the bulk of the active material host and in-plane mobilities ($\mu_{\text{in-plane}}$) parallel to a substrate are highly sensitive to local morphological features along their migration pathways. In general, the magnitudes of $\mu_{\text{out-of-plane}}$ and $\mu_{\text{in-plane}}$ are very different, in part because these carriers experience different morphological environments along their migration pathways. Suppressing the impact of variations in the morphological order/disorder on carrier migration remains an important challenge. While much is known about $\mu_{\text{in-plane}}$ and its optimization for devices, the current challenges are associated with $\mu_{\text{out-of-plane}}$ and its optimization for device performance. Therefore, this review is devoted to strategies for improving $\mu_{\text{out-of-plane}}$ in neat CP films and the implications for more complex systems, such as D:A blends which are relevant to OPV devices. The specific strategies discussed for improving $\mu_{\text{out-of-plane}}$ include solvent/field processing methods, chemical modification, thickness confinement, chemical additives, and different post-annealing strategies, including supercritical fluids. This review leverages the most recent fundamental understanding of mechanisms of charge transport and connections to morphology, identifying robust design strategies for targeted improvements of $\mu_{\text{out-of-plane}}$.

1 Introduction

Advances in theory, simulations, and experiment, together with improvements in processing and manufacturing, have enabled realization of the long-term goal for commercial use of conjugated polymer (CP)-based optoelectronic devices, such as organic photovoltaics (OPVs), organic light emitting diodes (LEDs), and organic field effect transistors (OFETs).^{1–14} The performance of these devices is largely dependent on the mobilities of charge carriers throughout the CP host, including external and internal interfaces, degree of structural order/disorder, and composition.¹ In organic LEDs, for example, the imbalance between hole and electron mobilities in the recombination layer is responsible for charge build-up, which impairs the external quantum efficiencies. In polymer FETs, charge carrier mobilities control switching speeds; in OPVs, the short circuit current, the fill factor, and therefore the power conversion efficiencies are also influenced by charge carrier mobilities. While it is well known that CP charge carrier mobilities are significantly impacted by chain packing and local variations of the morphology of the host,² an intimate understanding of the role of local morphological variations on carrier transport, and the development of effective strategies to control carrier mobilities to achieve high performance CP-based devices continue to pose vexing challenges. To date, apart from the molecular design and synthesis of next generation high carrier mobility molecules, attempts to control CP morphologies have been extensively explored, though improvements of out-of-plane transport specifically still lacks a coherent strategy.

Due to their hierarchical structures, the conformations of single polymer chains, chain segmental packing within aggregates/crystallites and amorphous domains, and interconnections between these domains, charge transport in CPs is characterized by multiple length scales and time scales. Charges migrate rapidly along the backbone of a single chain over nanometer length scales (i.e., conjugation length). For a planar (or straight) chain backbone, the adjacent p_z orbitals are parallel and electrons delocalize along consecutive π bonds. Defects (e.g., kinks, twists, and bends) reduce the effective conjugation length so the carrier mobility over longer length scales along the chain is reduced. An alternate view is that defects provide activation barriers to carrier migration, hence a reduction in mobility along the chain. π -stacking or π -aggregation occurs in CP hosts, which are inherently semicrystalline. Inter-chain migration requiring multiple hopping events, over length scales of tens of nm within aggregates/crystallite phases, is facilitated by interchain electronic coupling, though the coupling between the stacked layers is not as strong as coupling along the chain backbone. Moreover, the extent of order between the crystalline domains is not always perfect and is characterized by a paracrystallinity parameter, accessible using X-ray diffraction. Paracrystallinity therefore affects carrier mobility. Charge transport within an amorphous region is highly inefficient compared to ordered regions because of disruptions to both the conjugation lengths and the π - π -stacking organization. Hence, macroscopic transport throughout a CP host occurs by movement of charges from one ordered domain to another so the connectivity between the domains becomes the limiting factor, as discussed later.

Because of their transport anisotropy, challenges associated with the development of effective morphological design and processing strategies to achieve optimal device performance will differ based on the specific device application. For instance, Figure 1a shows that enhanced in-plane transport is required for OFETs and for certain sensors, whereas for OPVs, OLEDs, supercapacitors, and diodes, fast out-of-plane transport is desirable. To this end, engineering charge transport in preferred

¹ Department of Materials Science and Engineering, Biointerfaces Institute, University of Michigan, Ann Arbor, MI 48109, USA.

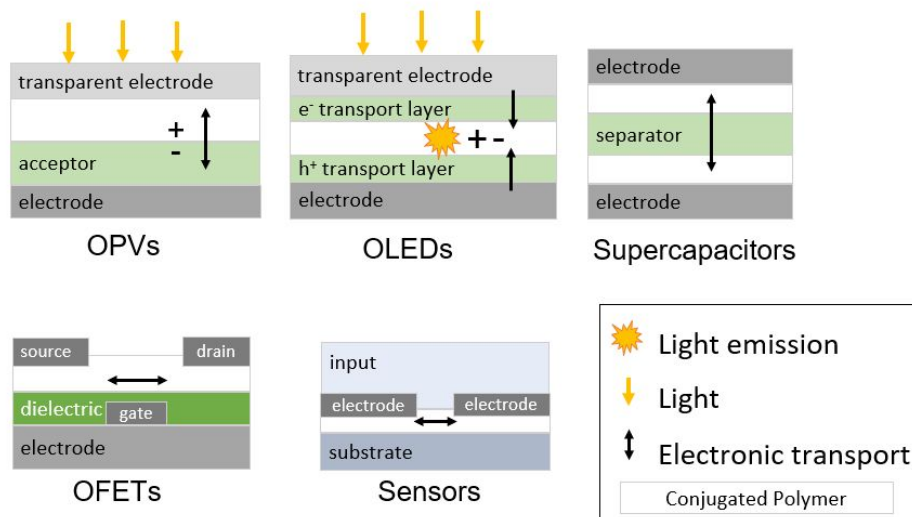
² Current address: Department of Materials Science and Engineering, Northwestern University, Evanston, IL 60201, USA.

³ National Renewable Energy Laboratory, 15013 Denver W Pkwy, Golden, CO 80401, USA.

*Email: pfgreen@umich.edu, Peter.Green@NREL.gov

[‡]These authors contributed equally to this work.

a) Electronic Transport in CP-based devices



b) Transport anisotropy in CPs

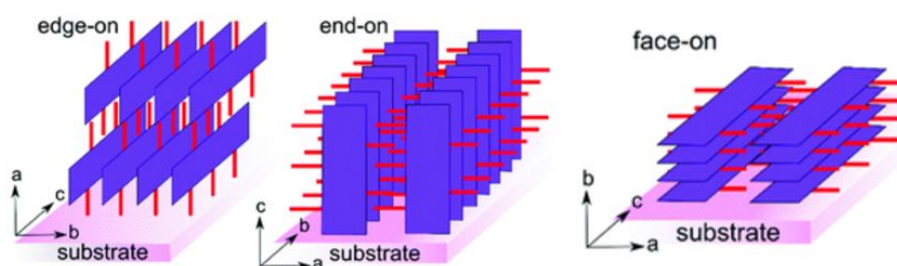


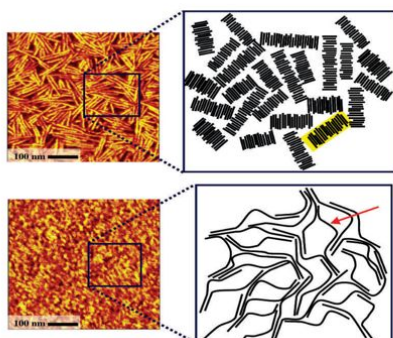
Figure 1. *Transport in conjugated polymer devices.* (a) Examples of conjugated polymer-based devices, from left to right: organic field effect transistors, organic photovoltaics, organic light-emitting diodes, sensors, and supercapacitors. The traditional direction of transport in these devices is shown with the black double arrow, and the conjugated polymer film is shown as the white layer. If there is light emission, this is shown with a yellow pom. (b) From left to right: edge-on, end-on ("chain-on"), and face-on conjugated polymer chain alignments are shown. The blue rectangles represent the main chain and red rectangles represent the side chains. (b) Reproduced from ref¹⁴ with permission from the Royal Society of Chemistry.

directions in devices is enabled by an understanding and control of CP charge migration anisotropy (see Figure 1b), as well as a fundamental understanding of morphological dependent mechanisms that control long-range (i.e., in- and out-of-plane) transport.¹⁵ Generally, enhanced charge transport in the in-plane direction, particularly relevant for OFETs, has been promoted by chain packing in the so-called "edge-on" direction (see Figure 1b). In this "edge-on" orientation, the main chain backbone direction of the CP as well as the π - π stacking direction align parallel to the substrate. Additionally, the side chains align perpendicular to the substrate, thereby enabling fast charge transport in the direction of conjugation. In the out-of-plane transport direction, however, the "edge-on" orientation is least preferred (typically the side chains are insoluble and therefore insulating) due to limiting carrier mobilities. The "face-on" and "chain-on" (also referred to as "end-on") orientations are more favored for the out-of-plane transport direction, because the π - π stacking direction in the "face-on" direction and the intrachain transport direction in the "chain-on" configurations facilitate rapid charge transport vertically. Notably, the "chain-on" orientation has enabled

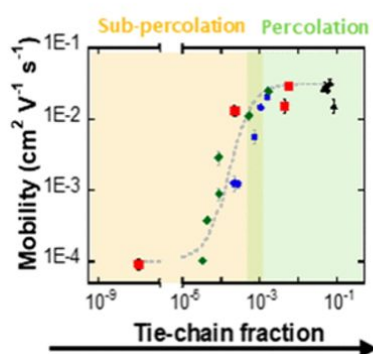
record mobilities in CPs (e.g., greater than $3.1 \text{ cm}^2 \text{ V}^{-1} \text{ s}^{-1}$ for poly-3-hexylthiophene (P3HT) as measured out-of-plane in nanopatterned devices by Skrypnichuk et al.¹⁵) and enhanced efficiencies upon integration into OPVs, as noted by Wang et al.¹⁶

The scientific literature is replete with discussions of in-plane mobilities ($\mu_{in-plane}$) of CPs,¹⁷⁻²⁰ as well as strategies, including external mechanical forces, molecular self-assembly, or substrates, to induce favorable CP orientations and improving $\mu_{in-plane}$.¹⁴ The CP chain orientations within a few nanometers of the dielectric substrate of a thin film transistor strongly influence, and enhance, the magnitudes of $\mu_{in-plane}$. Moreover, the carrier densities are highest in this region of the device because of the applied gate voltage. While much is understood about this mode of transport, the out-of-plane mobilities ($\mu_{out-of-plane}$), in contrast, are much more sensitive to the morphological disorder of CPs in the bulk and not as well understood. The problem is compounded by the fact that accurate measurements of $\mu_{out-of-plane}$ are comparatively difficult, and strategies to enhance $\mu_{out-of-plane}$ are more challenging due to their much lower carrier densities

a) MW-dependent morphology



b) Tie-chain dependent mobility



c) Charge percolation path

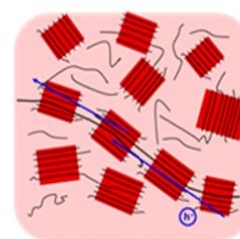


Figure 2. Role of tie-chains on charge transport. (a) Illustrations of CPs morphologies for low MW (top) and high MW (bottom) polymers. Low MW samples are composed of highly crystalline but isolated domains, whereas high MW samples are composed of smaller crystallites/aggregates connected via bridging chains, so called tie-chains (indicated by the red arrow). (a) Reproduced from ref²⁷ with permission from the American Chemical Society. (b) Field-effect mobilities of transistors comprising P3HT blends are plotted as a function of the tie-chain fraction. (c) Illustration of the percolating network of tie chains (blue) required to connect individual grains (red shaded regions) and achieve high carrier mobilities. (b) and (c) Reproduced with permission from ref²⁶ (<https://pubs.acs.org/doi/10.1021/acsmacrolett.8b00626>) with permission from the American Chemical Society. Further permissions related to the material excerpted should be directed to the American Chemical Society.

throughout the bulk. These magnitudes are strongly influenced by morphological details, over various length-scales, along their pathways.

Because the literature regarding out-of-plane transport in CP systems is limited and $\mu_{out-of-plane}$ is so highly coupled to morphological details and more importantly device performance, it is appropriate to write a review that discusses strategies to enhance transport specifically in the out-of-plane direction with particular relevance to optimizing the performance of devices including polymer diodes (i.e., single component CP system) and OPVs (i.e., two component CP system). As an illustrative example, the "ideal" OPV morphology consists of high purity nanoscale interconnected networks of donor and acceptor materials that themselves possess high carrier mobilities. Indeed, continued improvement of OPV efficiencies could be met by synthesizing and utilizing yet unexplored organic materials in which the transport is less sensitive to morphology, briefly discussed later; an alternative route is to leverage the literature that provides many strategies to fabricate high-purity, directional, and continuous pathways for enhanced charge transport in the out-of-plane direction.^{21–25} The latter is discussed in this review in the context of other factors, like domain phase purity, that contribute to device performance.

This review, appropriately, begins with a description of the current mechanisms that govern the migration of charge carriers in conjugated polymer hosts, in order to provide the context for illustrating the role of morphological details over different length scales, and time scales, on carrier mobilities. The magnitudes $\mu_{in-plane}$ and $\mu_{out-of-plane}$ can differ by orders of magnitude, in part due to the role of morphological details of the polymeric host. In single component CP systems, various strategies, including processing, chemical modification, thickness confinement, and controlling degree of disorder as

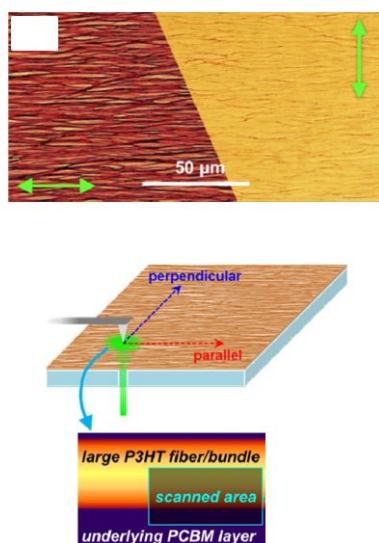
routes to enhance $\mu_{out-of-plane}$ are highlighted. To the best of our knowledge, this is the first review focusing strategies to improve out-of-plane transport in conjugated polymers, and more broadly organic semiconductors. In our prior review we described transport in both the in- and out-of-plane directions in thin CP films, but primarily focused on film thickness dependence of the out-of-plane charge transport and band bending phenomena. In this review, the focus is devoted exclusively to out-of-plane transport in CP films, morphological design and control, as well as measurements and methods to improve out-of-plane transport. Indeed, we noted during the writing of our previous review that insufficient attention has been devoted in literature to these issues. For a general discussion of transport in organic small molecule and polymeric semiconductors, readers are referred to a review by Fratini et al.⁷

Our review concludes with an example regarding two component D:A systems relevant to OPVs are briefly discussed, highlighting the role of morphological design in optimizing $\mu_{out-of-plane}$, as well as its contributing role in device performance. Overall, improving $\mu_{out-of-plane}$ in CP systems is challenging owing to difficulties in achieving vertical orientation of the CP backbone (i.e., fastest transport direction) and the sensitivity of transport to details of the degree of local morphological disorder. This review leverages the most recent fundamental understanding of charge transport, and the inherent connection to morphology, to offer robust design strategies for targeted improvement of $\mu_{out-of-plane}$ in CP systems.

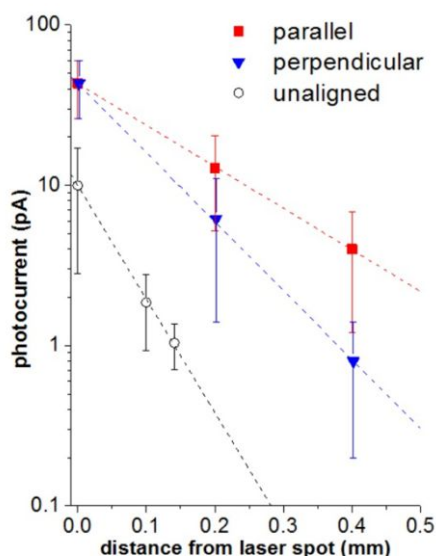
2 Mechanisms of charge transport in conjugated polymer hosts

2.1 Role of tie-chains, crystallite orientation and backbone rigidity of CPs

a) Long range carrier collection experimental set-up



b) Photocurrent as distance from laser spot



c) Proposed carrier migration pathway

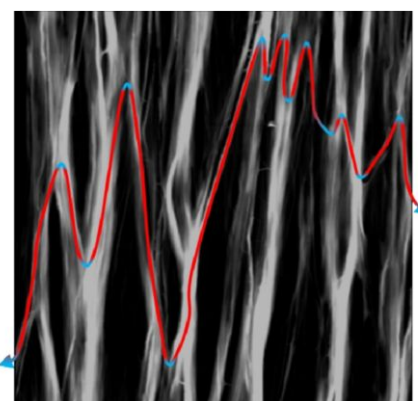


Figure 3. Role of crystallite orientation on charge transport of CPs. (a) Experimental set-up for long-range carrier collection investigation using p-AFM measurement. The laser illumination from below can be focused on a spot directly on the scan region or laterally displaced from it. The higher magnification (zoomed in) polarized optical microscopy image showed alignment of micrometer scale P3HT polymer fibers fabricated by epitaxy-directing solvent additive combined with an off-center spin-casting technique. The left-hand side and right-hand side of the image correspond to the same region viewed with polarizer oriented parallel and perpendicular (indicated by the green arrows) to the fiber alignment. (b) Photocurrents measured at varying distances from the laser spot for the parallel and perpendicular directions to the fibers in the aligned sample, and the unaligned sample where there was no distinction for parallel vs. perpendicular. (c) Proposed pathway for carrier migration perpendicular to the direction of alignment, overlaying the fiber morphology measured by AFM. (a)-(c) Reproduced and adapted with permission from ref²⁴ with permission from John Wiley and Sons.

The role of morphology on the migration of charge carriers throughout CP hosts is discussed in order to provide context to delineate key differences between in-plane and out-of-plane transport of charge carriers. It is noteworthy that experiments reveal that the magnitudes of $\mu_{in-plane}$ and $\mu_{out-of-plane}$ can differ by orders of magnitude, in some materials, depending on morphology, chemical constituents, device configuration, and measurement techniques. Currently, the most commonly accepted mechanism for macroscopic carrier migration in CPs suggest that carriers move from one ordered region to other ordered region along chain segments identified as tie-molecules.^{2,26} Motion along these tie molecules is rapid provided defects are minimal. Experiments reveal that field-effect mobilities of CPs are higher in samples with larger molecular weights (MWs), despite that fact that high molecular weight samples are characterized by a higher degree of disorder.^{27–31} However, it has been demonstrated that while the crystallites in short chain, low MW systems are more extended than their high MW chain analogs, the fraction of tie-molecules decreases with decreasing MW. This has the consequential

effect of reducing the number of tie-molecules between aggregates (see Figure 2a). Gu et. al quantified the effect of tie-chains on charge transport by investigating a series of blends P3HT molecules of differing MW fractions.²⁶ As shown in Figure 2b and 2c, a critical tie-chain fraction of 10^{-3} , calculated by using the Huang-Brown model, is necessary to enable appropriate macroscopic charge transport via charge percolation pathways.

Due to the high anisotropic transport characteristics, the alignment of crystallite domains is expected to have a profound impact on charge transport properties in CPs. Using an epitaxy-directing solvent additive 1,3,5-trichloro-benzene (TCB), combined with an off-center spin-casting technique, P3HT fibers with uniaxial in-plane alignment on the centimeter scale can be produced, as shown in Figure 3a. The samples are analyzed using novel experimental setup in which photoconductive atomic force microscopy (pc-AFM) is used to characterize bilayer planar heterojunction devices, assembled from phenyl-C61 butyric acid methyl ester (PCBM) acceptor, and both aligned and unaligned P3HT donor. It is evident from Figure 3b that by varying the relative positions of the laser spot

(site of carrier generation) and probe (site of hole extraction), devices with aligned P3HT fibers exhibit anisotropic and greatly enhanced long-range photocarrier transport, with nearly 10% of original photocurrent measured 0.4 mm from the laser spot along the direction parallel to the alignment. Notably, photocurrents collected in both parallel and perpendicular directions exhibited slower decay rates than the unaligned sample. The large current collected in the perpendicular direction can be explained by the availability of a proposed charge transport pathway in the direction perpendicular to the fibers, as illustrated in Figure 3c. These findings demonstrate the strong effect of orientation on directing charge transport in CPs.

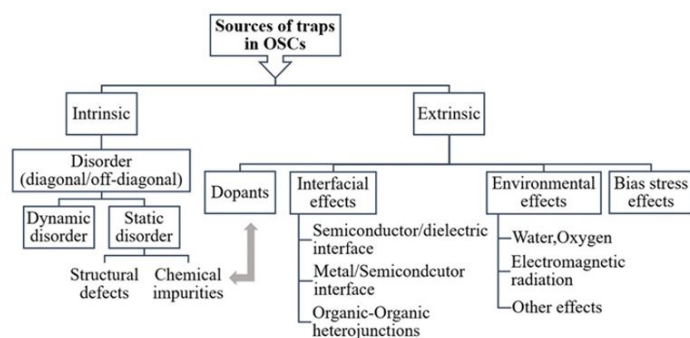
Early results from investigations of charge transport on polythiophene-based CPs, such as P3HT or poly[2,5-bis(3-tetradecylthiophen-2-yl)thieno[3,2-b]thiophene] (PBTBT), lead to a common misconception that increasing the long-range order, or degree of crystallinity, would naturally lead to an increasing charge mobility. However, a new generation of so-called donor-acceptor (D:A) CPs exhibit record values of carrier mobilities despite having seemingly high degrees of disorder and low degrees of crystallinity.^{3,32–34} In such cases, the enhanced mobilities have been achieved by increasing the planarity/stiffness of the monomer, thereby enhancing the conjugation lengths. A prominent example of these polymers is indaceno[1,2-b:5,6-b']dithiophene–benzothiadiazole (IDTBT) copolymer. Venkateshvaran et al. demonstrated that IDTBT exhibits a planar conformation in the solid state with a remarkably torsion-free backbone.³⁵ In the crystalline phase, the backbone

conformations in these disordered structures differ significantly between the PBTBT and IDTBT. Crystalline IDTBT adopts a wavy, yet remarkably planar, largely torsion-free backbone; the deviation from planarity remains exceptionally small with torsion angle of $5.26 \pm 4.0^\circ$. In contrast, PBTBT chains adopt a broader range of torsion angles ($27.2 \pm 14.6^\circ$) between thiophene and thienothiophene units. Importantly, even in a completely amorphous phase achieved by cooling low-density systems, IDTBT still retains its near-planar conformation, yet its density of states (DOS) is not significantly broadened. In contrast, PBTBT adopts conformations with larger spans in torsion angles and wider DOSs. The results provide an explanation for the surprisingly large mobilities in many recent D:A copolymers with a lower degree of crystallinity than P3HT or PBTBT.^{3,7,32–34,36,37}

2.2 Carrier traps and the influence on in- and out-of-plane transports in CPs

The weak intermolecular interactions in CPs, and for organic semiconductors (OSC) in general, make them susceptible to defect formation, resulting in localized states within the band gap that can trap charge carriers for different time scales. Charge carrier trapping is thus ubiquitous in CPs and has a profound impact on optoelectronic device. A detailed discussion about the underlying physics of traps and impact on electronic devices can be found in a recent review by Haneef et al.³⁸ For the purposes of this review, the physics of traps is briefly summarized. An electronic trap is defined as any imperfection in the semiconductor that creates localized

a) Sources of traps in OSCs



b) Trap DOS example

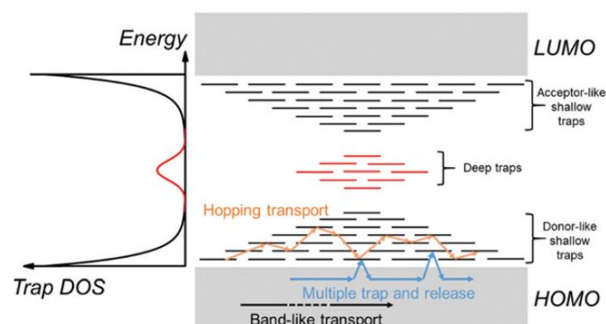


Figure 4. Sources of traps in organic semiconductors and the influence on general transport mechanism. (a) Sources of charge carrier traps in OSCs. (b) (left) The trap DOS showing shallow traps resulting from tail states (black) and deep traps (red) in the band gap. (right) Schematic spatial and energy diagram of an organic semiconductor (OSC) containing localized trap states in the band gap. Tail states are shown in black, while deep states are shown in red. Arrows represent different transport regimes possible in an OSC; band-like transport (black), multiple trap and release (blue) and thermally-activated hopping transport between localized states (orange). (a) and (b) Reproduced from ref³⁸ with permission from the Royal Society of Chemistry.

electronic states spatially distributed around the site of the imperfection and energetically distributed within the band gap of the semiconductor. Electronic traps, which are intrinsic and extrinsic, arise from multiple sources, as shown in Figure 4a.³⁸ Intrinsic traps originate primarily from structural, dynamic, or static disorder. Dynamic disorder is due to thermal motions of the molecules, leading to time-dependent variations in the site energies, whereas static disorder is time-independent, occurring only at locations where the defects are present. Dynamic disorder is particularly harmful for single crystal OSC device performance due to the formation of tail states, which trap charges.³⁹ Static disorder is more prominent in CPs where conformational defects such as kinks/twists are ubiquitous. While both dynamic disorder and static disorder introduce localized tail states in the band gaps of OSCs, static disorder is responsible for inducing additional in-gap states due to the presence of structural inhomogeneities.³⁸ Extrinsic traps, on the other hand, are associated with interfacial and environmental effects. Due to the presence of multiple layers in OSC devices, trapping at interfaces such as polymer/dielectric or metal/polymer has a profound impact on device performance. The most prominent example would be at the polymer/dielectric interface in OFET devices, where non-uniform topology,¹⁹ interface roughness,⁴⁰ or the adsorption of impurities such as water, oxygen or hydroxyl groups^{19,41} create charge carrier traps, which significantly hamper device

performance. Finally, traps in CPs can originate from environmental factors such as temperature, moisture (e.g., H₂O), ambient gases (e.g., O₂) and electromagnetic radiation (e.g., light, X-rays).³⁸

The influence of carrier traps on electronic structure and charge transport mechanism is illustrated in Figure 4b. Depending on their relative energetic positions in relation to the band edges (highest occupied molecular orbital (HOMO) or lowest unoccupied molecular orbital (LUMO) levels), traps can be shallow or deep. Shallow traps are located in the vicinity of the band edges, whereas deep traps reside further from the band edges. Importantly, a trap can capture and restrain a charge carrier temporarily until it is released back into the band by an external stimulus such as electric field, thermal energy, or a photon excitation. In the presence of traps, a charge carrier can move via a hopping mechanism, a multiple-trap and release (MTR) mechanism, or a band-like transport mechanism, depending on the density and energy position of traps. If the trap densities are high, trapped charge carriers can participate in transport through thermally activated hopping or tunneling from one localized state to another (see orange arrows in Figure 4b). If the trap densities are low, a band-like motion within delocalized states may occur (see black arrow in Figure 4b). In the intermediate case, charges moving within delocalized states are trapped by a localized shallow trap state in the band gap, then released back into the energy band by thermal energy; this

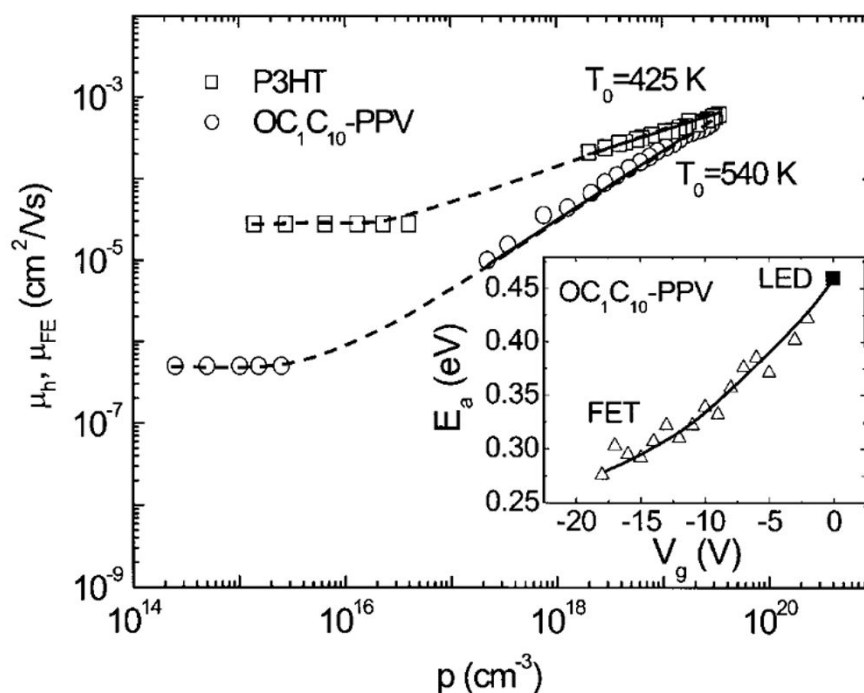


Figure 5. Carrier concentration dependent mobility. Carrier mobility as a function of hole density p in a diode (LED) and FET configurations for P3HT and OC1C10-PPV. The lower density regime represents diode measurement, whereas the higher density regime represents FET measurement. Inset: the activation energy of the mobility in the OC1C10-PPV based FET as a function of gate voltage (triangles), together with the activation energy of 0.46 eV as obtained from the diode at low density regime. Reproduced from ref⁴² with permission from the American Physical Society.

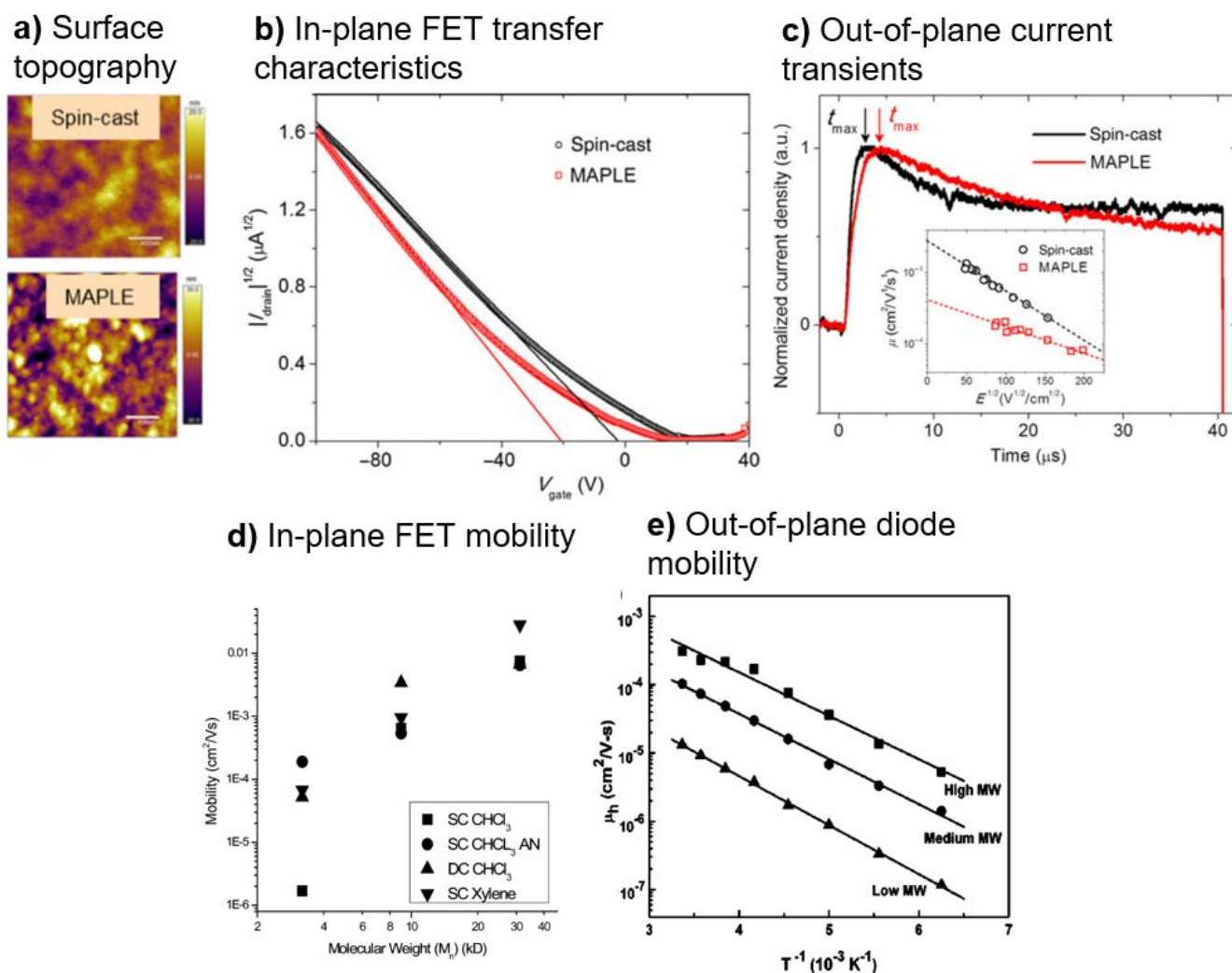


Figure 6. *Physics of in- and out-of-plane carrier transport.* (a) Surface morphology of spin-cast and MAPLE-deposited P3HT samples. (b) FET transfer characteristics of spin-cast and MAPLE-deposited samples. (c) Representative current transients measured by CELIV for spin-cast and MAPLE-deposited P3HT films at ramping rate $A = 25,000$ V/s. The inset shows the electric field dependence of out-of-plane carrier mobilities. (a)-(c) Reproduced and adapted from ref⁴³ with permission from Springer Nature. (d) MW dependent μ_{FET} of P3HT samples fabricated using different solvents and casting method: SC CHCl_3 : spin-casted using CHCl_3 , SC CHCl_3 AN: Spin-casted using CHCl_3 and then annealing, DC CHCl_3 : Drop-casted using CHCl_3 , SC Xylene: Spin-casted using xylene. (d) Reproduced from ref²⁷ with permission from the American Chemical Society. (e) Temperature dependent out-of-plane mobility $\mu_{\text{out-of-plane}}$ of P3HT samples at 3 different MWs: Low MW (2.89 kDa), medium MW (9.72 kDa) and high MW (31.1 kDa). (e) Reproduced from ref⁴⁷ with permission from AIP Publishing.

is called multiple trap and release (MTR) (see blue arrows in Figure 4b). Deep traps have a negligible probability of being thermally excited thus often act as recombination centers for charge carriers reducing their overall lifetime, which is deleterious to the performance of OPVs. Due to the strong dependence of carrier transport on trap density, carrier concentration is expected to play a crucial role in transport mechanisms in CPs. This leads to the dependence of carrier mobility on device configurations and transport direction, which is discussed below.

2.3 In-plane and out-of-plane carrier transport in conjugated polymer hosts

The influence of carrier concentration on carrier mobility in different device configurations was demonstrated by Tanase and coworkers.⁴² In this pioneering study, the authors measured $\mu_{\text{in-plane}}$ and $\mu_{\text{out-of-plane}}$ in the same materials (P3HT and poly(2-methoxy-5-(3',7'-dimethyloctyloxy)-p-phenylene vinylene (OC_{10} -PPV)) using FET and diode configurations, respectively. As shown in Figure 5, the experimental hole mobilities extracted from both types of devices, for a single

polymeric semiconductor, can differ by up to 3 orders of magnitude. This significant difference in part originated from the strong dependence of the hole mobility on the charge carrier density. The carrier densities for $\mu_{in-plane}$ measurements in FET configurations are much higher than for the case for $\mu_{out-of-plane}$ measurements in diode configurations. Larger carrier densities are responsible for lower activation energies (see inset of Figure 5) and therefore larger magnitudes of $\mu_{in-plane}$ in the case of FET measurements, compared to $\mu_{out-of-plane}$, extracted from diode (LED) measurements.

In another series of studies, Green and coworkers investigated the influence of morphological disorder on $\mu_{in-plane}$ and $\mu_{out-of-plane}$ of P3HT samples using FET and current extracted by linearly increasing voltage (CELIV).^{43,44} The CELIV technique is described in the next section. The authors utilized a vacuum fabrication technique, matrix-assisted pulsed laser evaporation (MAPLE), to fabricate P3HT samples that possessed higher degrees of morphological disorder compared to samples fabricated using the traditional spin-casting method. The highly

disordered morphologies of the MAPLE-deposited samples were characterized surface topography measurements (see Figure 6a) and a series of spectroscopy and X-ray analyses.^{43,44} The more disordered morphologies of the MAPLE-deposited samples are manifested in the higher subthreshold regime of FET transfer current measurement data; see Figure 6b for a typical example. Surprisingly, the $\mu_{in-plane}$ of the MAPLE-deposited sample is even higher than its spin-cast analogs, indicated by the steeper slope in the linear regime in the transfer characteristics. For octadecyltrichlorosilane (OTS)-treated substrates, the $\mu_{in-plane}$ of MAPLE and spin-cast samples were 8.3×10^{-3} and $5.5 \times 10^{-3} \text{ cm}^2\text{V}^{-1}\text{s}^{-1}$, respectively. To measure the $\mu_{out-of-plane}$, the authors employed the CELIV technique;⁴⁵ the current versus time data are shown in Figure 6c. Based on the raw CELIV data, the time corresponding to the peak of the transient current (t_{max}) is longer for the MAPLE-deposited sample, indicating a lower $\mu_{out-of-plane}$.⁴⁵ The MAPLE-deposited sample also exhibits a pronounced broadening of the transient current, indicative of more dispersive transport than

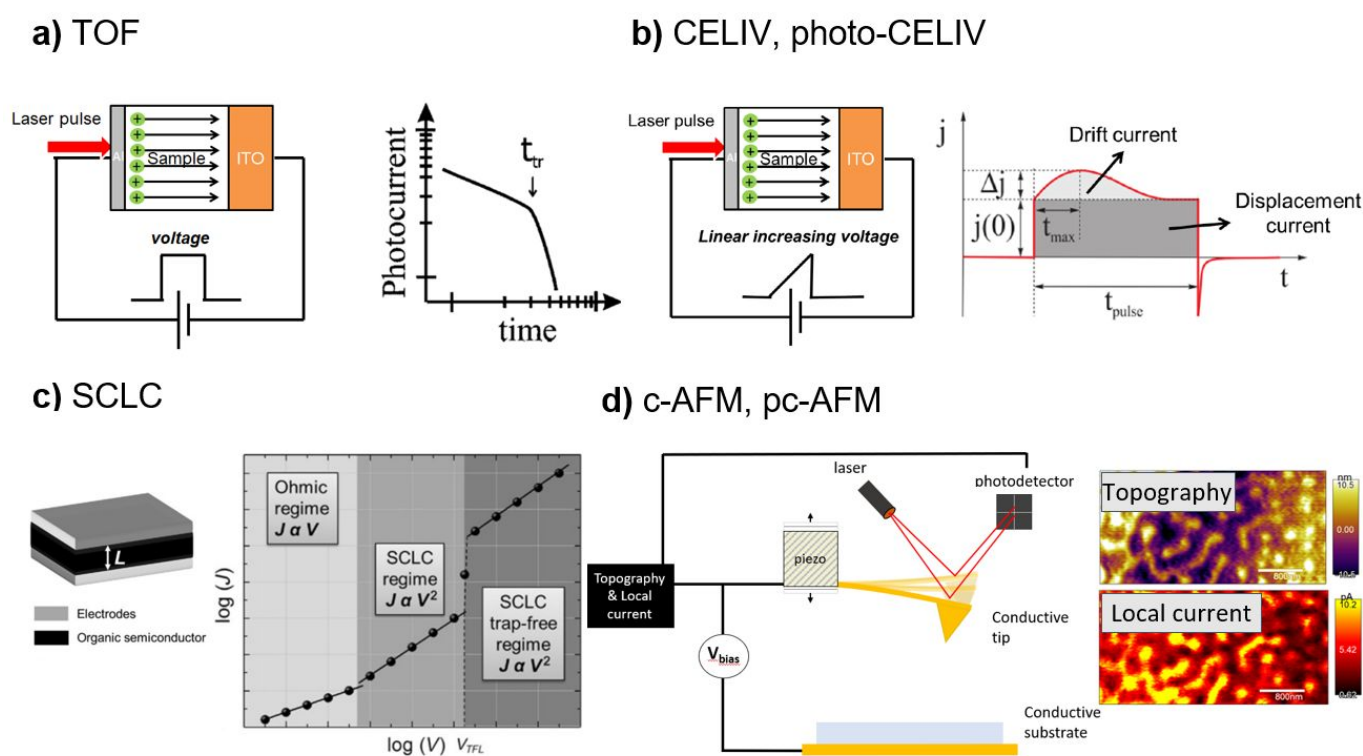


Figure 7. Overview of common techniques to measure out-of-plane transport. (a) Time of flight (TOF). *Left*: Sample set-up for TOF measurement. *Right*: Typical transient current response in TOF measurement. (b) Carrier extraction by linearly increasing voltage (CELIV) and photoinduced CELIV (photo-CELIV). *Left*: Sample set-up for CELIV/photo-CELIV measurements. *Right*: Typical transient current response in CELIV/photo-CELIV measurement. (b, right) Reproduced and adapted from ref⁵⁹ with permission from John Wiley and Sons. (c) *Left*: Schematic representation of the capacitor-type configuration used for SCLC measurement. *Right*: Typical charge limited current $\log J$ - $\log V$ behavior or CPs consisting of 3 main regimes: Ohmic regime ($J = \sigma/L \times V$), trap-containing SCLC regime and trap-free SCLC regime ($J \sim V^2$). (c) Reproduced and adapted from ref⁶⁸ with permission from Elsevier. (d) Conductive, photoconductive-AFM (c-AFM, pc-AFM) measurement. *Left*: experimental set-up and demonstration of c-AFM, pc-AFM working principles. *Right*: Exemplary topography and local current images at the same position of P3HT/PS blend. The scale bar is 800 nm (unpublished data).

the spin-cast sample; this is consistent with more structural disorder and a larger density of trap states. In addition to the lower zero field mobilities exhibited by the MAPLE sample compared to its spin-cast analog ($4.1 \times 10^{-4} \text{ cm}^2\text{V}^{-1}\text{s}^{-1}$ versus $2.7 \times 10^{-3} \text{ cm}^2\text{V}^{-1}\text{s}^{-1}$), the electric field (E) dependencies of mobilities, shown in inset of Figure 6c, reveal a weaker E dependence on $\mu_{\text{out-of-plane}}$ in the MAPLE-deposited sample. The weaker E dependence of $\mu_{\text{out-of-plane}}$ is indicative of higher degree of energetic order in MAPLE sample as rationalized within the framework of the Gaussian disorder model (GDM) proposed by Bässler.⁴⁶ The extent to which morphological disorder impacts $\mu_{\text{in-plane}}$ and $\mu_{\text{out-of-plane}}$ highlights the challenges in improving $\mu_{\text{out-of-plane}}$ in CPs due to the inevitable structural disorder in CPs.

The fundamental differences between in-plane and out-of-plane transport behaviors are also evident from MW dependent charge transport studies. As shown in Figure 6d, McGehee and coworkers²⁷ demonstrated that increasing the MW of P3HT has a significant impact on the $\mu_{\text{in-plane}}$ of the polymer measured by FET configuration, regardless of processing conditions. The $\mu_{\text{in-plane}}$ was found to increase by 3 to 4 orders of magnitude going from a P3HT sample of 2.9 kDa to a sample of 31.1 kDa. The same authors in a separate study investigated the temperature dependence of $\mu_{\text{out-of-plane}}$, measured by SCLC in P3HT at 3 different MW: 2.9 kDa (low MW), 9.7 kDa (medium MW) and 31.1 kDa (high MW).⁴⁷ As illustrated in Figure 6e, over a range of temperatures (160 K – 300 K) and MWs, the $\mu_{\text{out-of-plane}}$ increases with MW. Additionally, the activation energies for carrier transport extracted from Arrhenius plots were found to decrease gradually from 143 meV to 126 meV, as the MW increased. The MW-dependent behaviors exhibited by $\mu_{\text{out-of-plane}}$ and μ_{FET} are similar, though the dependence of $\mu_{\text{out-of-plane}}$ on the MW is not as strong as that of μ_{FET} in the plane of the film. This observation is consistent with the notion that carrier densities in the diode configurations are much lower than for FET geometries. This again highlights the challenges associated with improving $\mu_{\text{out-of-plane}}$ in CPs in the presence of traps, and more importantly the role of morphology.

3 Out-of-plane transport measurements

3.1 Overview

It is evident from the foregoing that unlike the $\mu_{\text{in-plane}}$ s, the $\mu_{\text{out-of-plane}}$ s manifest the outcomes of various processes associated with morphological details of the CP. Generally, because of the way they are measured, the $\mu_{\text{in-plane}}$ s manifest the migration of carriers within nanometers of a substrate where the chain backbones are typically preferentially oriented within the plane, in the midst of higher carrier densities, for the typical transistor measurement configuration.^{18,48} On the other hand, different measurement techniques are used to extract $\mu_{\text{out-of-plane}}$ s, but they each have particular strengths and weaknesses associated with the mechanisms that enable the mobilities to be extracted. It will be evident that some are more sensitive to certain details of the morphology at certain length-scales than others. Therefore, it is important to know not only the magnitudes of the mobilities, but also the technique used to extract them.

3.2 Time-of-flight (ToF) Spectroscopy

The Time of Flight (ToF) technique is arguably one of the straightforward and most widely used methods for extracting mobilities⁴⁹ and has been used to measure out-of-plane mobilities of OLED and OPV materials.^{50–53} A schematic representation of ToF measurement set-up together with a typical photocurrent response determined from experiment are shown in Figure 7a. In the ToF method, the CP sample is sandwiched between two electrodes. Importantly, one of the two electrodes must be transparent/semitransparent to allow the transmission of light. A laser pulse is applied to the surface of the material through this transparent/semitransparent front electrode, generating a “sheet” of charge carriers. The width of this layer depends on the absorption coefficient of the CP at the laser wavelength, which is typically less than 100 nm. An E field is simultaneously applied across the device to draw the thin layer of charge carriers from the front electrode to the back electrode. As this sheet of charges reaches the back electrode, a drop in the photocurrent is observed and a characteristic plateau and a “kink” at the transit time (t_{tr}) is observed in the photocurrent transient, as illustrated on the right side of Figure 7a. The carrier mobility is then calculated using the following equation:

$$\mu = \frac{d^2}{t_{\text{tr}}V}$$

Here, d is the sample thickness and V is the applied voltage. In general, the utilization of ToF is limited to several requirements: (i) the dielectric relaxation time should be larger than t_{tr} ; (ii) d should be significantly larger than the width of the generated carrier sheet making ToF measurement on sample thinner than 1 μm problematic; (iii) injection-blocking contacts are required to prevent unwanted carrier injection from perturbing E .⁵⁴

3.3 CELIV and photo-CELIV

The CELIV technique has been more recently utilized for the characterization of charge transport in CPs and other OSCs (see Figure 7b).^{55–59} As shown in Figure 7b, the sample geometry and experiment setup are similar to that of the ToF technique. However, in contrast to ToF measurements, CELIV utilizes a triangle voltage (hence the term linearly increasing voltage) instead of a square voltage to drive carriers from the front electrode to the back electrode. Depending on the intrinsic carrier density, a laser pulse might be required to generate carriers for CELIV measurements (this is the so-called derivative photo-CELIV technique); the CELIV technique is otherwise viable, provided a sufficient density of carriers is generated within the sample. Unlike TOF, CELIV is appropriate for samples with thickness of several hundreds of nanometers, or even less than 100 nm.^{60,61} A typical current transient in a CELIV/photo-CELIV measurement is shown on the right side of Figure 7b. The current transients exhibit maxima at t_{max} during the early stages of the application of the electric field. The CELIV model assumes that the diffusion current is negligible, so the current transient has two major contributions: the displacement current ($j(0)$)

due to the geometric capacitance of the sample and the drift current (Δj) represents the charges extracted from the film. The time at which the total current transient reaches a maximum (t_{max}) is used to calculate μ using the following equation.⁵⁸

$$\mu = \frac{2d^2}{3At_{max}^2(1 + 0.36\frac{\Delta j}{j(0)})}$$

Note that in the case of photo-CELIV, the photogenerated carrier concentration distribution and hence light absorption profile needs to be taken into account, requiring a modified formula to calculate the carrier mobility as pointed out by Juška *et al.*^{60,62} The CELIV technique not only measures mobilities in thinner films than can be measured using the ToF technique, but it also utilizes much weaker fields. Moreover, charge transport in materials with high bulk conductivities can be characterized.

3.4 Space-charge-limited current (SCLC) techniques

Space-charge-limited current (SCLC) theory was first developed by Mott and Gurney in 1940 for single-carrier injection in a trap-free insulator.⁶³ Since then it has been adopted for mobility measurements in a wide variety of OSCs.^{64–67} In an SCLC measurement, an OSCs of thickness, L , is sandwiched between two electrodes; the evolution of the current (J) with the applied voltage (V) is recorded (see Figure 7c). The SCLC J - V dependence, is characterized by three regimes, as illustrated in Figure 7c. The first regime is the low V , ohmic regime where the current increases linearly with the voltage according to Ohm's law ($J \sim V$). At higher fields, the current becomes space-charge limited (hence the name SCLC), which is reflected in a quadratic dependence on the applied voltage ($J \sim V^2$) and further divided into two parts. In the first part of the SCLC regime, a fraction of the injected carriers is trapped and the steady-state SCL current is reduced by a factor (ϑ), which represents the ratio between the concentration of free (n_f) and total (n_{tot}) charge carriers present in the device. As the voltage increases, traps are gradually filled, resulting in an increase in the density of free charge carriers. At the trap-filling limit voltage (V_{TFL}), all traps are filled and the current rises abruptly, leading to the SCLC trap-free regime. The carrier mobility is usually measured in trap-free SCLC regime using the following equation:⁶⁸

$$J = \frac{9}{8} \times \mu \epsilon \epsilon_0 \frac{V^2}{L^3}$$

Similar to CELIV, SCLC has advantages over ToF because of its ability to measure mobilities in films as thin as 100 nm, which is the relevant thickness for most of the optoelectronic devices. However, SCLC has certain drawbacks, including the need for careful selection of the electrodes (1 injection and 1 blocking contact electrodes); additional fitting parameters are usually required for materials that exhibit field dependence mobilities.⁵⁴

3.5 Conductive (c)-atomic force microscopy (AFM), pc-AFM

c-AFM and pc-AFM are local contact scanning probe measurements performed on generally smooth thin film OSC samples supported by conductive substrates.^{69–73} In these measurements, information about the topography is collected simultaneously with the conductivity, as a conductive probe is scanned across the surface of the sample (see Figure 7d). The topography is monitored by a laser reflected from the back of the tip onto a photodiode. For the c-AFM measurement, no illumination is provided to the sample; a bias is applied between the tip and conductive substrate. With regard to the pc-AFM measurement, a laser provides photoexcitation (often through the bottom of a transparent conductive substrate). Typically, a preliminary scan is performed in the "dark" (i.e., no illumination by laser or lamp) to determine the current offset required to correct the dark current to zero, and this offset is maintained for all subsequent measurements on the sample. An advantage of (p)c-AFM is that topographical features can be correlated with local current; this has proven useful for understanding the role of grain boundaries in photoexcited samples⁷⁴ and

visualizing different phases in D:A materials.^{23,72} Local current-voltage (I - V) curves can also be extracted, enabling characterization of local electronic properties of OSCs, though a notable disadvantage of c-AFM is that the complex geometry of the measurement prohibits using the standard Mott-Gurney law to fit the data; thus a semi-empirical model must be used to extract mobilities from c-AFM that match well with flat electrode geometry.^{70,71,75} Exemplary topographical and local current images at the same position of P3HT/PS blend are shown in Figure 7d.

4 Methods to improve the out-of-plane carrier mobilities in single component CP systems

4.1 Overview

In the following section, various strategies used to enhance $\mu_{out-of-plane}$ of CPs are described. The name of the polymer, magnitudes of $\mu_{out-of-plane}$, film thicknesses, processing and measurement techniques of each CP discussed are summarized in Table 1 and provided in order in which they are discussed in the review.

4.2 Improvement of $\mu_{out-of-plane}$ via control of molecular orientation

It is understood that carrier transport in conjugated polymers is highly anisotropic, with rapid transport occurring along the backbones of the chains and along certain chain stacking directions (see Figure 1b). This provides insight into specific transport pathways that might be designed within the morphology of a polymer in order to optimize carrier mobilities. The scientific literature is replete with examples illustrating the influence of processing on morphology/polymer chain orientation and in-plane transport characteristics of CPs. In the case of polythiophene-based CPs such as P3HT, edge-on orientation, where the π -stacking direction is oriented in the lateral direction, is usually more favorable for in-plane transport compared to face-on orientation in which carriers inevitably

Table 1 Summary of CPs and out-of-plane mobility or (photo)current extracted using reference transport control strategies discussed in this review. Examples provided in order they are discussed in the review.

CPs	$\mu_{out-of-plane}$ ($\text{cm}^2\text{V}^{-1}\text{s}^{-1}$)	Film thickness	Transport measurement method	Transport control strategies	refs
P3HT	2.7×10^{-3} (spin-cast), 4.1×10^{-4} (MAPLE)	~100 nm	CELIV	Spin-cast vs MAPLE	Li ⁴³ , Dong ⁴⁴
P3HT	1.33×10^{-5} (2.89 kDa) 1.13×10^{-4} (9.72 kDa) 3.3×10^{-4} (31.1 kDa)	~100nm	SCLC	MW control	Goh ⁴⁷
P3HT	$(0.7 - 3.5) \times 10^{-3}$ (before rubbing) $(4 - 6) \times 10^{-3}$ (after rubbing)	4-10 μm	ToF	Mechanical rubbing	Kajiya ^{93,94}
P3HT	10^{-4} (smooth sample) (3 - 10) (nanopatterned sample)	380 nm	SCLC, c-AFM (~30-40 pA)	nanopatterning	Skrypnichuk ¹⁵
PTBn (n=1-7)	$(2.6-7.7) \times 10^{-4}$	~100 nm	SCLC	Backbone/side-chain modification	Liang ^{95,96}
P3BT and P3BT-F17	4.2×10^{-5} (P3BT), 1.6×10^{-3} (P3BT-F17)	N/A	SCLC	Chain-end modification	Ma ⁹⁷
P(NDI2OD-T2)	$\sim 10^{-2}$ (RR, casted and annealed), $\sim 10^{-4}$ (RI, as cast)	N/A	SCLC	RR modification and change processing condition	Steyrleuthner ⁹⁸
P3HT	7.1×10^{-5} (thickness = 80 nm), 8.6×10^{-4} (thickness > 700nm)	80 nm – 5 μm	CELIV, impedance, ToF	Thickness confinement	Yang ⁹⁹ Huang ⁶¹
PBDTTT-C	2×10^{-4} (thickness = 60 nm), 7×10^{-4} (thickness > 100nm)	60 nm – 1 μm	Photo-CELIV, ToF	Thickness confinement	Dong ⁶⁰
DPP-BTz	0.2	220 nm	SCLC	Reduce disorder	Nikolka ¹⁰⁰

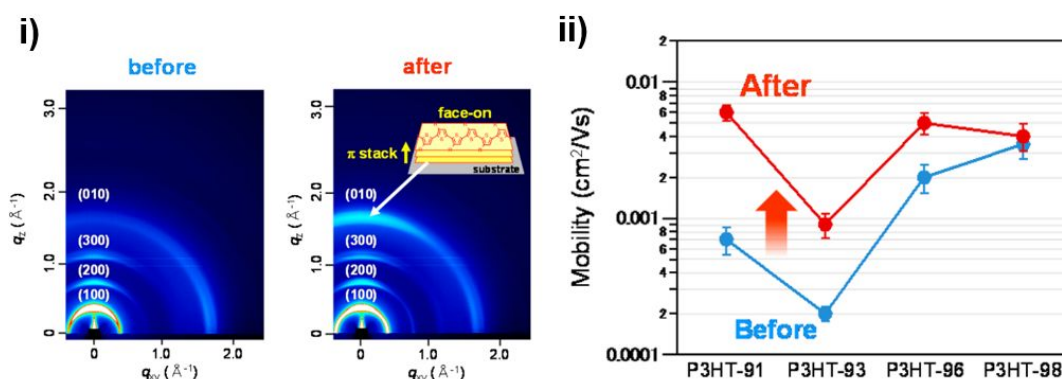
have to hop through the insulating side-chain direction to move in the in-plane direction.⁷⁶ In addition, $\mu_{in-plane}$ of P3HT has been

shown to improve ~5 fold as a result of processing the samples for better in-plane alignment of polymer backbone.⁷⁷ Several CPs such as pBTTT or diketo pyrrolo-pyrrole (DPP)-based CPs exhibit values of $\mu_{in-plane}$ from 0.1 - 1 $\text{cm}^2\text{V}^{-1}\text{s}^{-1}$, which is an order

of magnitude larger than that of P3HT, due in part to the remarkable in-plane alignment of the polymer backbones.⁷⁸⁻⁸⁰

Moreover, significant enhancement in $\mu_{in-plane}$ has been demonstrated by aligning the polymer backbone along the transport direction using various methods including off-center spin-casting,^{24,81} epitaxy alignment,^{82,83} mechanical rubbing,⁸⁴ Langmuir-Blodgett technique,⁸⁵ nanoconfinement,⁸⁶ among other techniques.^{5,87-90} $\mu_{in-plane}$ as high as 50 $\text{cm}^2\text{V}^{-1}\text{s}^{-1}$ has been

a) Mechanical rubbing



b) Fabricating nanopatterns

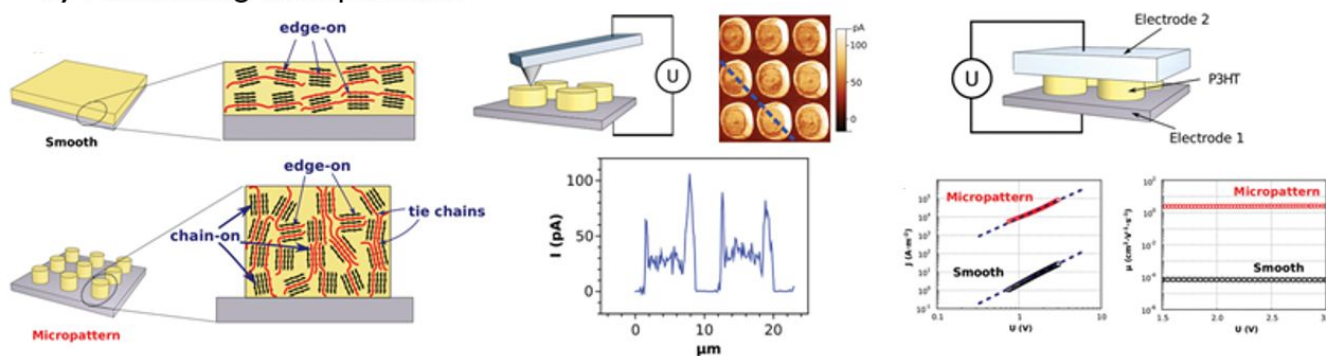


Figure 8. Processing methods to enhance $\mu_{\text{out-of-plane}}$ (a) Improving $\mu_{\text{out-of-plane}}$ through mechanical rubbing method. (i) Comparing GIWAXS patterns of P3HT films before and after rubbing clearly shows the enhanced intensity of the π -stacking (010) peak, indicating the increasing fraction of $\mu_{\text{out-of-plane}}$ -favored face-on orientation after mechanical rubbing. (ii) The $\mu_{\text{out-of-plane}}$ before and after mechanical rubbing, for P3HT samples with different regioregularity. (a) Reproduced and adapted from ref⁹³ with permission from the American Chemical Society. (b) Improving $\mu_{\text{out-of-plane}}$ through nanopatterning. (left) Illustrations of structures of smooth and micropatterned P3HT samples. (middle) 3D schematics of the macroscopic measurement, where a potential difference U is applied between the conductive substrate and an electrode lying on top of the film, and the current flowing vertically through the film is measured. (right) Plots of macroscopic vertical current density (J) in smooth and micropatterned films, showing space-charge limited transport in both samples, and vertical charge-carrier mobility calculated from J - U curves. (b) Reproduced and adapted from ref¹⁵ with permission of John Wiley and Sons.

realized in CPs by coupling high mobility polymers with nanogrooved-substrate-assisted macroscopic alignment of polymer backbones.^{8,91}

Based on successful control of CPs orientation for improving $\mu_{\text{in-plane}}$ to date, it is expected that similar orientation control processes could potentially improve $\mu_{\text{out-of-plane}}$ of CPs as well. As opposed to in-plane transport where edge-on orientation is the most favorable configuration, chain-on and face-on orientations where the fast transport directions along the polymer backbone and π -stacking are oriented in the out-of-plane direction is desired. Achieving those configurations, however, is more challenging because edge-on orientation is

usually more thermodynamically favorable than face-on orientation.⁹² Aligning CPs vertically, as in the chain-on orientation, is an even more daunting task due to the tendency of the polymer backbone to lie parallel to the substrate. Here, we summarize several methods for orientational control of CP domains for improving $\mu_{\text{out-of-plane}}$ through processing, chemical modification, and thickness-confinement.

4.2.1 Processing strategies

To control molecular orientation for enhanced $\mu_{\text{out-of-plane}}$, Kajiya and co-workers applied a mechanical rubbing method on solution-casted P3HT films.^{93,94} Grazing incidence wide angle X-ray scattering (GIWAXS) patterns before and after mechanical

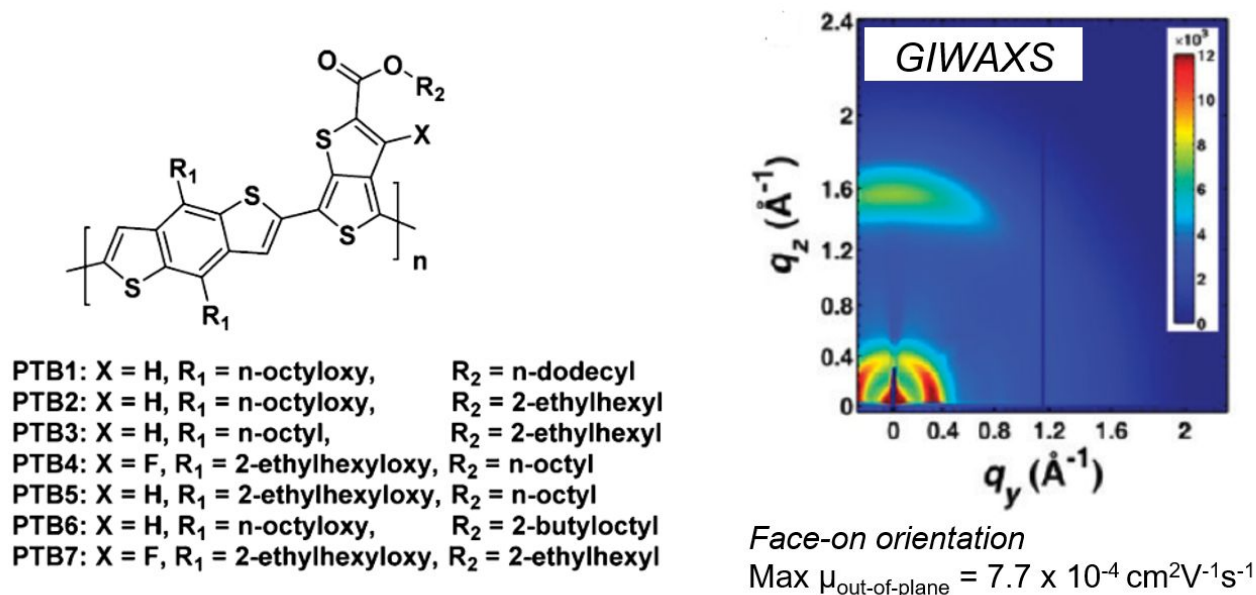


Figure 9. Orientation control via backbone/side-chain modification. Chemical structures of PTB family polymers, together with representative GIWAXS pattern of PTB7. The maximum $\mu_{\text{out-of-plane}}$ for the PTB series is $7.7 \times 10^{-4} \text{ cm}^2\text{V}^{-1}\text{s}^{-1}$. (left) Reproduced from ref¹¹ with permission of the American Chemical Society. (right) Reproduced from ref¹⁰¹ with permission of the American Chemical Society.

rubbing shown in Figure 8a(i) revealed an increase in the fraction of face-on crystallites as evidenced by the enhanced intensity of the (010) peak in the out-of-plane direction. Consequently, the $\mu_{\text{out-of-plane}}$ after rubbing was found to increase as much as eightfold in P3HT samples with 91% regioregularity (RR) (see Figure 8a(ii)), becoming almost equal to the $\mu_{\text{out-of-plane}}$ of 98% RR sample. The largest enhancement was achieved for the low RR film, which had the most disordered structure before rubbing, and was attributed to the low elastic modulus of the lower RR P3HT. Thus, the rubbing of P3HT significantly increased ordering within the structure,

which facilitated carrier migration in the out-of-plane direction.

In another study, Skrypnichuk et al. demonstrated a three order of magnitude enhancement in $\mu_{\text{out-of-plane}}$ in an undoped P3HT film through orientational control by using a microstructured substrate.¹⁵ As shown in Figure 8b, the authors discovered that in a regular smooth sample, the polymer crystallite adapted edge-on lamellae orientation with chain backbone and π -stacking in the plane of the film, resulting in poor vertical charge transport. On the other hand, the micropatterned sample fabricated by a nanoimprinting method having a combination of chain-on and randomly oriented crystallites, with vertical chain alignment and tie-chains (red lines) connecting crystallites vertically, promote a very efficient charge transport mechanism and high hole mobility in the vertical direction inside the micropatterns. The orientation induced by micropatterning was due to a confinement effect and the flow of materials during the fabrication process. This

produces very efficient charge transport from the bottom to the top of the pillars and enables record high mobilities of $10.6 \text{ cm}^2\text{V}^{-1}\text{s}^{-1}$ as confirmed by both J-U (see Figure 8b) and c-AFM measurement.

4.2.2 Chemical modification

Arguably, polythiophene-based CPs such as P3HT are the most widely-used and investigated classes of CPs for optoelectronic applications. However, despite their frequent use as model testbeds for understanding structure/transport relationship, the $\mu_{\text{out-of-plane}}$ of P3HT remains relatively low, on the order of $10^{-5} - 10^{-4} \text{ cm}^2\text{V}^{-1}\text{s}^{-1}$ near room temperature.⁹⁹ The low $\mu_{\text{out-of-plane}}$ of P3HT is in part due to the unfavorable edge-on orientation of polymer crystallites, for reasons discussed above. Motivated largely by a need for higher OPV efficiencies, new CPs with stronger absorption profiles (lower bandgaps), better D:A energy alignment and larger $\mu_{\text{out-of-plane}}$ s are desired. Major achievements arise from the breakthrough of D:A mixtures, leading to highly efficient BHJ PSCs.¹¹ A significant breakthrough was made when the PTB polymers, which consist of alternating electron-rich benzodithiophene (BDT) units and electron-deficient thienothiophene (TT) units, were introduced (see Figure 9, left).^{95,101-103} By moving from the thiophene unit in P3HT to a more planar and flat backbone in PTB series, the polymer crystallites/aggregates in PTB adopted preferential face-on orientations with the π - π stacking direction nominally in the out-of-plane direction, as evidenced by their GIWAXS patterns (see Figure 9, right). The largest $\mu_{\text{out-of-plane}}$ values achieved in the in PTB series were $7.7 \times 10^{-4} \text{ cm}^2\text{V}^{-1}\text{s}^{-1}$ in

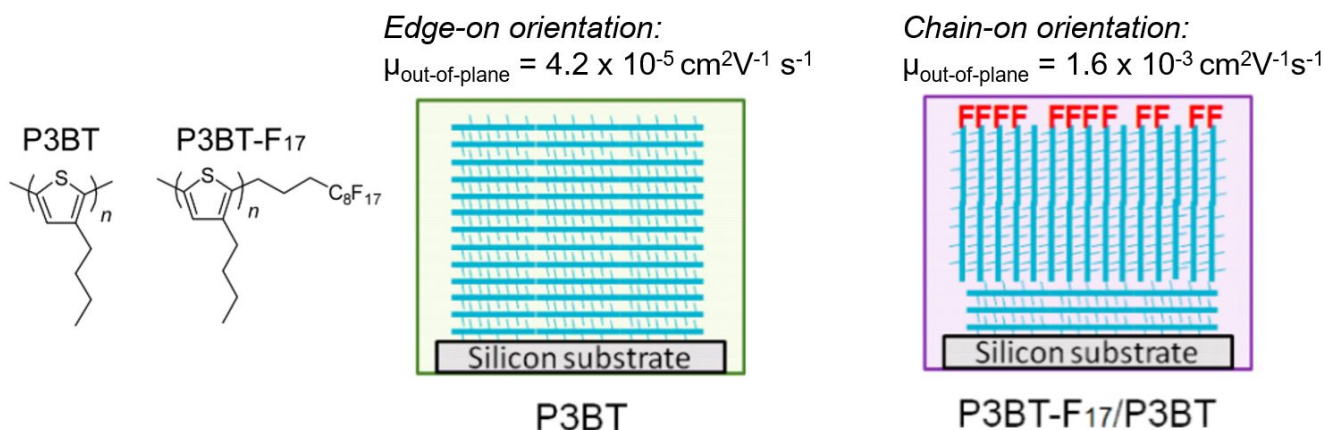


Figure 10. *Orientation control via end group modification.* Chemical structures of P3BT and P3BT-F17, which the end group chemistry is the difference between the two. Illustration of chain orientation in P3BT and P3BT/ P3BT-F17 bilayer samples. The $\mu_{\text{out-of-plane}}$ for the two configurations are $4.2 \times 10^{-5} \text{ cm}^2\text{V}^{-1} \text{ s}^{-1}$ and $1.6 \times 10^{-3} \text{ cm}^2\text{V}^{-1} \text{ s}^{-1}$, respectively. Reproduced and adapted from ref⁹⁷ with permission from the American Chemical Society.

PTB4.¹⁰⁴ While this is a rather modest increase in $\mu_{\text{out-of-plane}}$ compared to P3HT, the results showed that backbone/side-chain modification can lead to favorable molecular orientations and thus enhancements in $\mu_{\text{out-of-plane}}$.

In another notable study, Ma and co-workers modified the end group chemistries of poly(3-butylthiophene) (P3BT) to achieve end-on (chain-on) orientation and improve $\mu_{\text{out-of-plane}}$ via simple spin-casting method.⁹⁷ In general, achieving a vertical orientation of the CP backbone remains challenging; it requires sophisticated processing methods such as nano-imprinting, as discussed in the prior section. As seen in Figure 10, the authors fabricated the so-called surface-segregated monolayers (SSMs) using P3BT with one chain end functionalized with a 1H,1H,2H,2H,3H,3H-perfluoroundecyl group (P3BT-F17). The fluoroalkyl group at the chain end of P3BT-F17 self-segregated to the surface, which aligned the P3BT backbone perpendicular to the surface and produced the maximum surface coverage. In addition, because of the high crystallinity of P3BT, the surface orientation induced polymer chains in the bulk of the film to adopt the same orientation. The charge transport properties in the direction normal to the substrate were investigated using SCLC and exhibited a nearly 2 order of magnitude improvement in $\mu_{\text{out-of-plane}}$, from $4.2 \times 10^{-5} \text{ cm}^2\text{V}^{-1} \text{ s}^{-1}$ in P3BT and $1.6 \times 10^{-3} \text{ cm}^2\text{V}^{-1} \text{ s}^{-1}$ P3BT-F17. The results demonstrate that end-group modification is a powerful method to achieve end-on orientations, hence fast out-of-plane transport in CPs.

Finally, changing RR has been shown to be another successful method for modifying morphological structure and $\mu_{\text{out-of-plane}}$ of CPs. Earlier in section 4.2.1 we showed that post-processing is impacted by changing RR of CPs. In this section we show how the RR directly influence morphology and out-of-plane transport properties of CPs. Steyrlleuthner et al. studied the effect of RR on morphology and $\mu_{\text{out-of-plane}}$ of an n-type CP,

poly{[N,N'-bis(2-octyldodecyl)-1,4,5,8-naphthalenediimide-2,6-diyl]-alt-5,5'-(2,2'-bithiophene)} [P(NDI2OD-T2)].¹⁰⁵ The authors synthesized both the conventional RR- and regioirregular (RI)-P(NDI2OD-T2) (see Figure 11, left), solution-processed under different conditions and studied molecular packing behaviors and the corresponding out-of-plane charge transport characteristics of both polymers. P(NDI2OD-T2) is a high mobility n-type CP that largely exhibit face-on orientations, with exceptional in-plane ordering, as illustrated in Figure 9c, top right.¹⁰⁶ P(NDI2OD-T2) also demonstrated exceptionally high n-type $\mu_{\text{out-of-plane}}$ values, close to $3.5 \times 10^{-3} \text{ cm}^2\text{V}^{-1} \text{ s}^{-1}$, measured using the ToF and SCLC techniques.⁹⁸ Structural characterization using GIWAXS (see Figure 11, top right) coupled with other spectroscopic techniques revealed that different solvent and annealing conditions have a strong influence on the orientation of the polymer chains with respect to the substrate. RR-P(NDI2OD-T2) adopts face-on orientations when casted from chlorobenzene (CB) and edge-on orientations when casted from chloronaphthalene:xylene mixtures (CN:Xyl). Further annealing both CB and CN:Xyl below the melting point increased the crystallinity of each sample while maintaining the same overall crystallite orientation. RI- P(NDI2OD-T2), on the other hand, was less sensitive to processing, exhibiting a highly disordered structure regardless the solvent or annealing conditions. The SCLC electron mobility of P(NDI2OD-T2) (see Figure 11, bottom right) strongly correlated with the degree of out-of-plane ordering of the polymer backbone. The highest mobilities approaching $10^{-2} \text{ cm}^2\text{V}^{-1} \text{ s}^{-1}$ were achieved in annealed CB-casted RR-P(NDI2OD-T2) where the polymer sample had the highest degree of crystallinity and face-on orientation. The smallest mobilities, close to $10^{-4} \text{ cm}^2\text{V}^{-1} \text{ s}^{-1}$, were exhibited by RI-P(NDI2OD-T2) at all conditions, consistent with structural characterization. These findings highlighted the

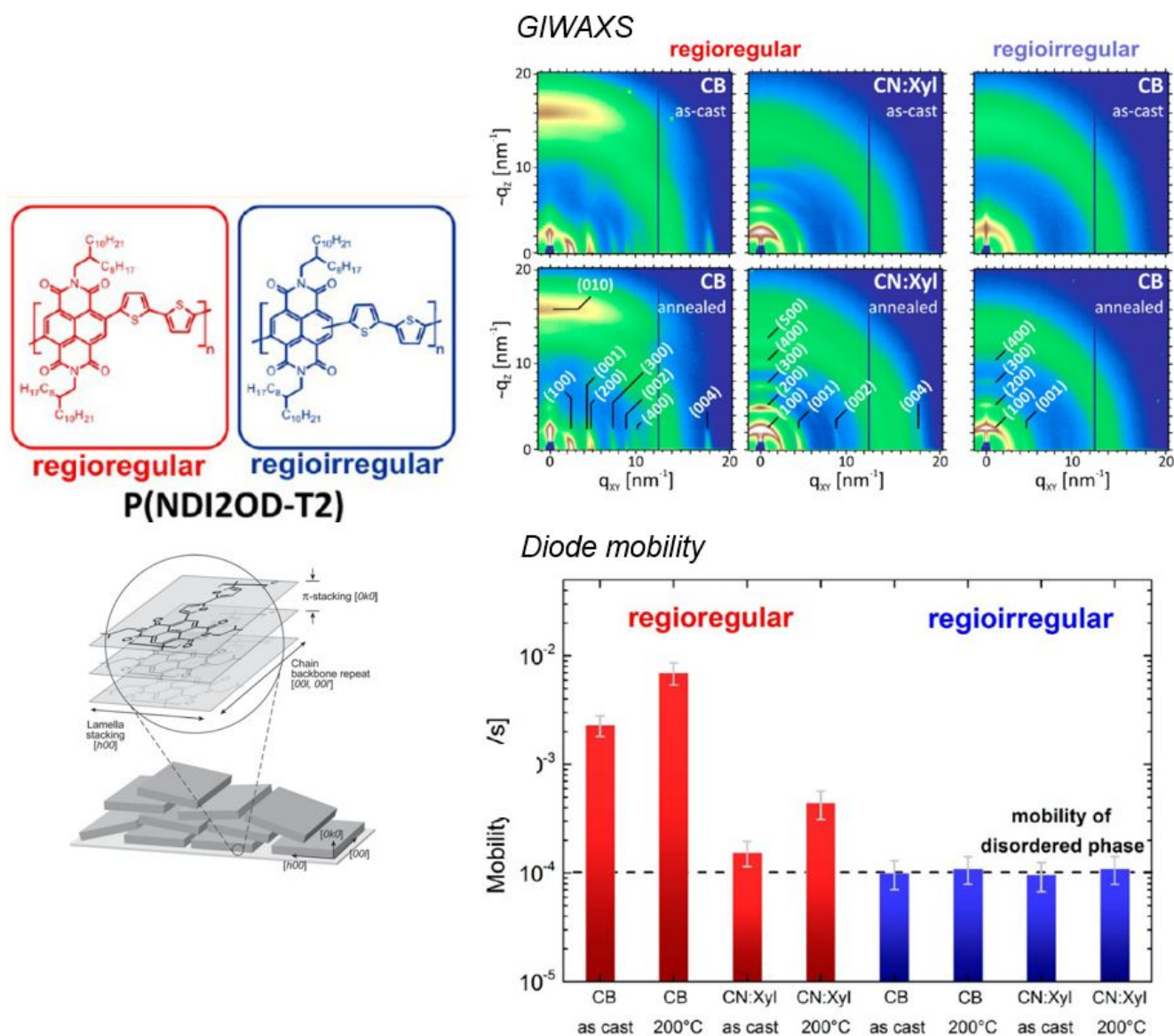


Figure 11. Orientation control via regioregularity modification. Chemical structures of RR- and RRA-P(NDI2OD-T2), together with the schematic molecular alignment in P(NDI2OD-T2) thin film. GIWAXS patterns of regioregular (RR)- and regiorregular (RI)-P(NDI2OD-T2) at different processing/annealing conditions. Diode mobility of different RR- and RI-P(NDI2OD-T2) samples. (top left, right) Reproduced from ref¹⁰⁵ with permission from the American Chemical Society. (bottom left) Reproduced from ref¹⁰⁶ with permission from John Wiley and Sons.

important role of controlling RR and processing conditions on out-of-plane transport in CPs.

4.2.3 Thickness confinement

While ideas on thickness confinement in this section were discussed in our prior review,¹ they are summarized here because the data in Figure 12 represent the only thickness dependent out-of-plane mobilities of which we are aware. This information, moreover, sets the context to introduce the strategies that enhance out-of-plane transport in polymeric systems. In CP thin films, the existence of external interfaces

(polymer/substrate and polymer/air) can significantly influence charge transport.

A substrate has the effect of preferentially changing the orientation of the ordered phase in polymer systems, as well as inducing a higher degree of local order, a fact well-known for ordered block copolymer lamellae.^{107,108} For the case of semi-crystalline CP thin films, depending on how the interface is prepared, the nature of the interactions between the polymer and the substrate could enhance or decrease the local degree of crystallinity of the samples, change molecular orientation and thus affect charge transport.¹ Therefore, one of the

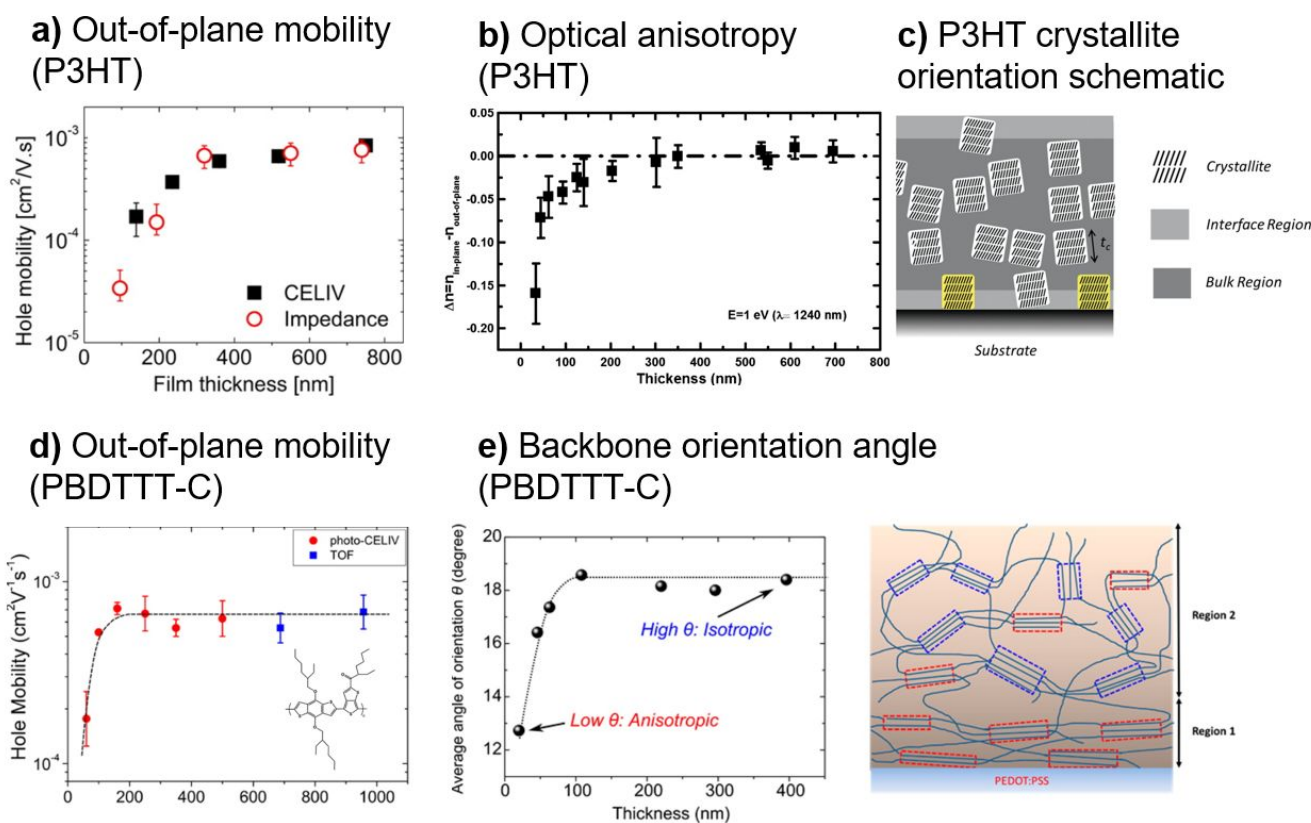


Figure 12. *Orientation control via thickness confinement.* (a) Thickness dependent $\mu_{out-of-plane}$ of P3HT samples measured by both CELIV and impedance spectroscopy techniques. (a) Reproduced from ref⁹⁹ with permission from the American Chemical Society. (b) Optical anisotropy of P3HT samples measured by spectroscopic ellipsometry as a function of film thickness. (b) Reproduced from ref⁶¹ with permission from the American Chemical Society. (c) Illustration of CP crystallite orientation in the bulk and in the interfacial regions of a thin film. Reproduced from ref¹⁰⁹ with permission from John Wiley and Sons. (d) Thickness dependent of poly[4,8-bis((2-ethylhexyl)-oxy)benzo[1,2-b:4,5-b']dithiophene-2,6-diyl-alt-4-(2-ethylhexan-1-one)thieno[3,4-b]-thiophene-2,6-diyl] (PBDTTT-C) $\mu_{out-of-plane}$ measured by both photo-CELIV and TOF (Chemical structure of PBDTTT-C shown in inset). (e) Left: Backbone orientation angle as a function of film thickness. Right: Illustration of PBDTTT-C's morphological structure at the region near (region 1) and far away (region 2) from the substrate. (d) and (e) Reproduced from ref⁶⁰ with permission from the American Chemical Society.

strategies for enhancing $\mu_{out-of-plane}$ is to control chain orientations by taking advantage of polymer/substrate interactions.

In a series of investigations, utilizing CELIV, impedance spectroscopy and TOF, Green and co-workers showed that the $\mu_{out-of-plane}$ in P3HT is a strong function of film thickness, increasing from $3 \times 10^{-5} \text{ cm}^2\text{V}^{-1}\text{s}^{-1}$ in 100 nm thick samples to ca. $10^{-3} \text{ cm}^2\text{V}^{-1}\text{s}^{-1}$ in samples thicker than 700 nm (see Figure 12a). Measurements of the index of refraction anisotropy as a function of film thickness, using spectroscopic ellipsometry, reveal that the changes in the anisotropy exhibit the same trends in thickness dependence as $\mu_{out-of-plane}$, shown in Figure 12b, consistent with the notion that the increase in the fraction of different crystal orientations that favor more rapid out-of-plane carrier transport. Specifically, as the films became thicker, the fraction of face-on aggregates increased, giving rise to the

increase in carrier mobility. X-ray diffraction studies of the structure of P3HT films, by others, also show an increase in face-on orientation with increasing film thickness, thereby corroborating the findings (see Figure 12c).^{92,109}

In a related study, Dong et al. investigated the thickness dependent structure and charge transport of the D:A copolymer PBDTTT-C (chemical structure shown in inset of Figure 12d).⁶⁰ Using a combination of CELIV and ToF, the authors measured the $\mu_{out-of-plane}$ of PBDTTT-C samples with film thickness ranging from 60 to 1000 nm, and discovered that, for all thicknesses, $\mu_{out-of-plane}$ showed a negative dependence on E with a strength quantified by the Pool-Frankel coefficient (or slope) (θ). The negative dependence of μ on E was rationalized within the framework of Gaussian disorder model, indicating the existence of significant positional disorder due to the semicrystalline nature of the samples. The zero-field $\mu_{out-of-plane}$ ($\mu_{E=0}$,

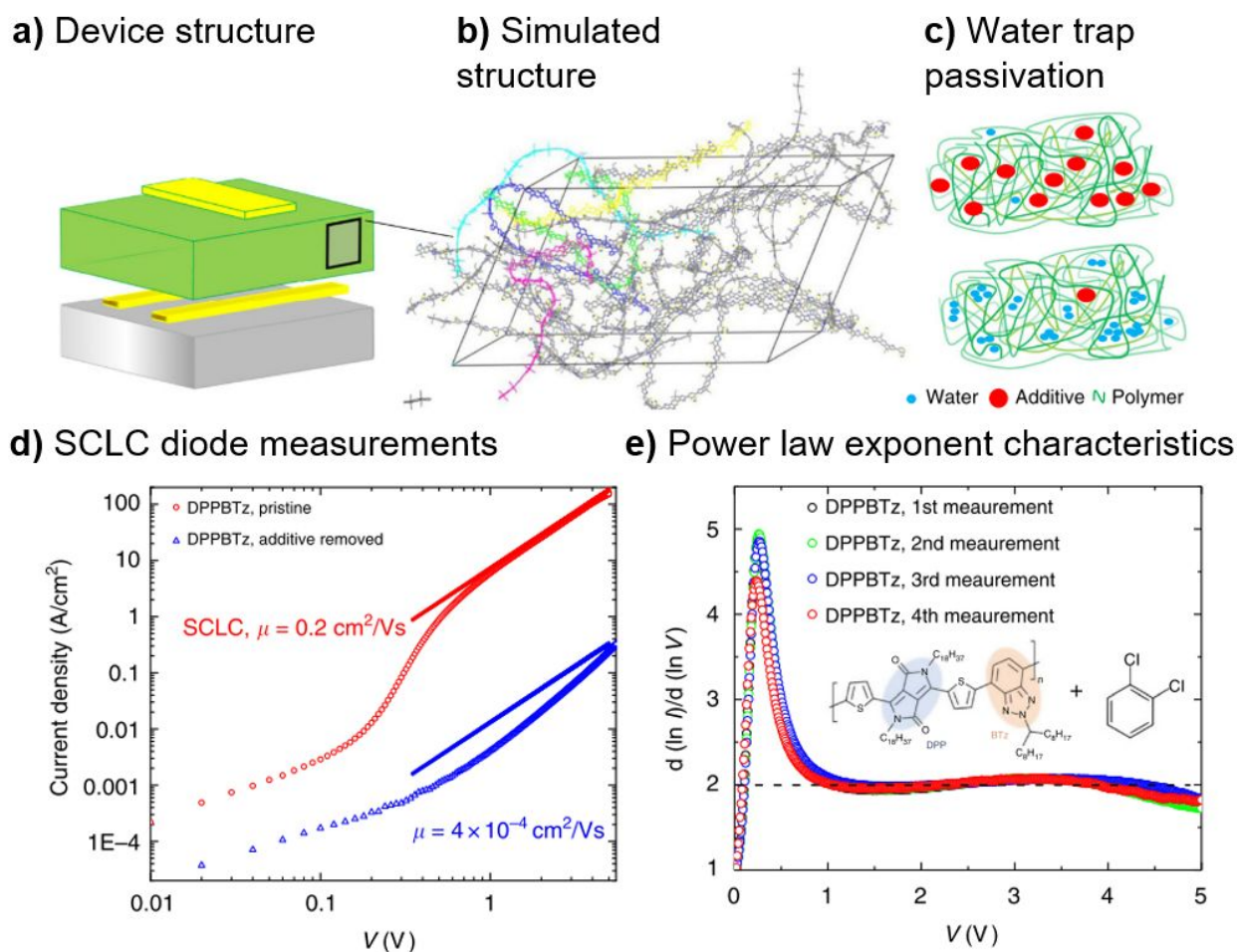


Figure 13. Enhancing $\mu_{\text{out-of-plane}}$ via controlling the degree of disorder. (a) Device structure of SCLC measurement. (b) Simulated structure of a high-mobility amorphous polymer. (c) Passivation of water-induced traps in the polymer sample through the use of additives (red). Removing additives leaving waters that disrupt charge transport (d) Exemplary hole-only SCLC diode characteristics of DPP-BTz. The $\mu_{\text{out-of-plane}}$ before and after solvent removal are $0.2 \text{ cm}^2\text{V}^{-1}\text{s}^{-1}$ and $4 \times 10^{-4} \text{ cm}^2\text{V}^{-1}\text{s}^{-1}$, respectively. (e) Power law exponent of the SCLC characteristics extracted during repeated measurements. The chemical structure of DPPBTz as well as the additive (residual 1,2-dichlorobenzene (DCB) solvent) is also show. (a)-(e) Reproduced from ref¹⁰⁰ with permission from Springer Nature.

extrapolated from $\log \mu$ vs $E^{1/2}$ plot) exhibited strong thickness dependence associated with substrate-induced local morphological orientations throughout the film thickness. Using spectroscopic ellipsometry, the authors calculated the average orientation angle (ϑ) of the polymer backbone as a function of film thickness. As shown in Figure 12e, ϑ increases with film thickness and saturates beyond 100 nm. This result indicates that the polymer aggregates (crystallites) at and near the substrate adopt orientations that are preferentially parallel to the substrate (region 1) but becomes more random as the distance away from the substrate increases (region 2), as the effect of the substrate decreases (see Figure 12e). Therefore, the increase of the carrier mobility with film thickness is due to the preferential out-of-plane orientation of polymer backbones

within the polymer crystallites near the substrate. Taken together, the results demonstrate the critical role of substrate-induced molecular orientation on out-of-plane transport in CPs and optimum $\mu_{\text{out-of-plane}}$ can be realized by choosing appropriate film thicknesses. A more detailed summary of the influence of polymer/substrate interaction on charge transport of CPs can be found in our recent review.¹

4.3 Improvement of $\mu_{\text{out-of-plane}}$ via control of degree of disorder

Decades of research in the field of CPs have improved their charge transport properties of dramatically by exploring the wealth of viable chemical structures and processing conditions. Today, in-plane FET mobility of CPs consisting alternating electron-rich and electron-deficient units such as

indacenodithiophene (IDT), diketopyrrolo-pyrrole (DPP), naphthalenediimide, cyclopentadithiophene, or isoindigo regularly exceeds $1 \text{ cm}^2\text{V}^{-1}\text{s}^{-1}$.^{7,36,37} However, despite the improvement in the field of OFET, achieving similar values of value for $\mu_{\text{out-of-plane}}$ still remains a significant challenge. This is due largely to the low charge carrier concentration in the bulk which is typically on the order of $10^{15}\text{--}10^{16} \text{ cm}^{-3}$, leading to trap-limited charge transport. Even in the highest performing D:A CPs, the $\mu_{\text{out-of-plane}}$ rarely exceeds $10^{-3} \text{ cm}^2\text{V}^{-1}\text{s}^{-1}$.^{98,110} Therefore, improving $\mu_{\text{out-of-plane}}$ requires a method to suppress the degree of disorder within the CP samples.

To suppress disorder and improve $\mu_{\text{out-of-plane}}$, Nikolka et al. investigated the origin of trap states in a high FET mobility, low-disorder D:A polymer poly[[2,5-bis(2-octadecyl)-2,3,5,6-tetrahydro-3,6-diketo-pyrrolo[3,4-c]pyrrole-1,4-diyl]-alt-(2-octylnonyl)-2,1,3-benzo-triazole] (DPP-BTz).¹⁰⁰ DPP-BTz is a D:A CP with a high field-effect mobility of $2 \text{ cm}^2\text{V}^{-1}\text{s}^{-1}$ in spin-coated films and up to $6.7 \text{ cm}^2\text{V}^{-1}\text{s}^{-1}$ in uniaxially aligned film.¹¹¹ The authors proposed that out-of-plane transport is limited by water-induced trap states and that their concentration can be reduced through incorporating small molecular additive dichlorobenzene (DCB) into the polymer film. To study the influence of DCB additive on out-of-plane transport, the author fabricated gold-contact diode structures (see Figure 13a). The authors then compared these “additive devices” to “devices without additive” that are subjected to either longer annealing at $90 \text{ }^\circ\text{C}$ for 1 h or extended storage in vacuum, which both removes the residual solvent from the film (see Figure 13b and c). The I-V characteristics measured by SCLC methods of both “additive devices” to “devices without additive” are shown in Figure 13d. The device without DCB (blue curve) exhibited a low current density and the observed voltage dependence is significantly stronger than what is expected from Mott–Gurney’s law (indicated by the blue solid line), suggesting trap limited transport mechanism across the entire applied voltage range. In contrast, the additive device exhibits a much higher current density and a textbook-like SCLC behavior, having Ohmic regime at low voltage, a steep trap-filling regime between 0.2 and 0.6 V, and a trap-free, SCLC regime above 1 V in which the J–V characteristics follow Mott–Gurney’s law and a very high, field-independent SCLC mobility of $0.2 \text{ cm}^2\text{V}^{-1}\text{s}^{-1}$ is extracted (red line). This demonstrated a record mobility for a diode based on a solution-processed CP film. Monitoring the power of the current density dependence on voltage (see Figure 13e) showed excellent stability over the course of several hours of measurement. The results suggested that high mobility, nearly trap-free vertical transport could be achieved in CP diodes through judicious control of degree of traps and disorder within the polymer sample.

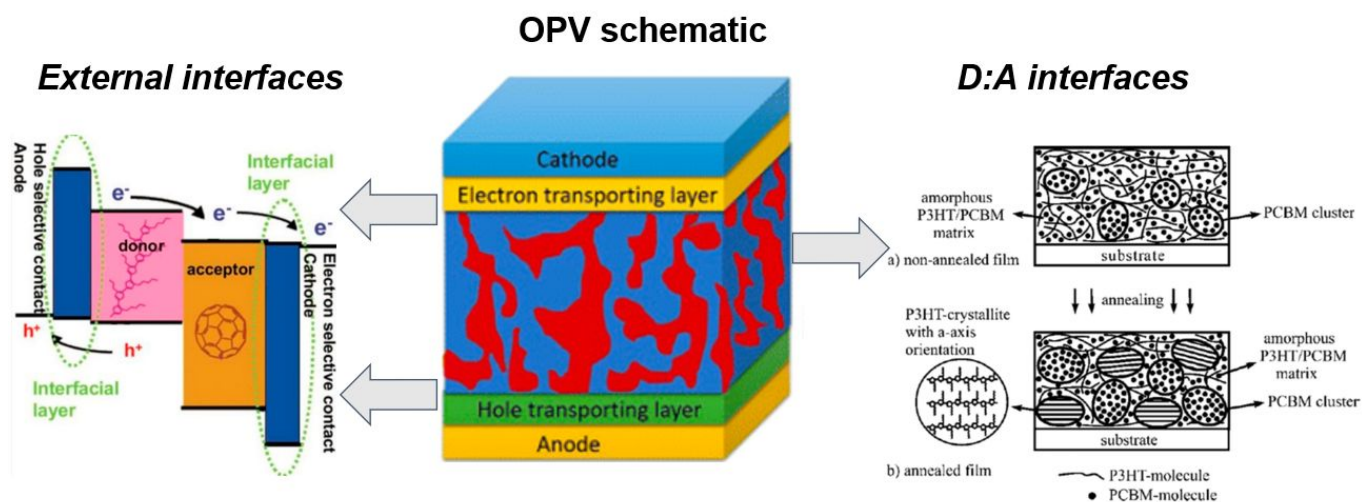
5 Strategies to improve carrier mobilities in D:A material systems

5.1 Overview of OPV devices: interfacial and morphological impacts

It is evident from the foregoing that microstructural features influence the values of $\mu_{\text{in-plane}}$ and, more profoundly $\mu_{\text{out-of-plane}}$; the latter is of particular relevance to power conversion efficiencies (PCEs) of D:A based OPV devices. Generally, in OPVs, events occurring at internal interfaces between donors and acceptors and at external interfaces at electrode layers play the central role in the performance of OPVs (see Figure 14)¹¹² - carrier mobilities and charge recombination fundamentally influence the short-circuit current (J_{SC}), open circuit voltage (V_{OC}) and the fill factors; $(\text{FF})(V_{\text{OC}})(J_{\text{SC}})=\text{PSC}$.

An exciton, after its formation, migrates to the D:A interface where it dissociates, with the electron subsequently migrating through the acceptor phase and hole remaining with the donor phase. These charge carriers migrate to their respective electrodes where they are harvested (see Figure 14).¹¹ The size, the compositional purity, the pathways, and the morphology of the migration pathway of a domain phases collectively determine out-of-plane transport and $\mu_{\text{out-of-plane}}$. When excitons are formed their diffusion distances should be small to minimize the probability of recombination on their way to the D:A interface. A small domain size in a D:A blend is associated with a large internal interfacial D:A area (and vice versa), which facilitates the generation of a large carrier density. Small domain sizes are associated with longer migration pathways, and therefore a greater influence of the microstructure on the mobility of a carrier and an increased recombination probability, before harvesting at an electrode. Additionally, the purity of the of the domain phase is important because recombination occurs at higher rates (which reduces the FF) in impure regions. An additional point is that the breadth of the interface between the donor and the acceptor is on the order of nanometers, so efforts should be made to not only maximize the domain size but also domain purity; this would be consistent with minimizing the size of the interfacial region. In general, optimal domain sizes are on the order of $\sim 10\text{--}40 \text{ nm}$.^{11,113} As an example, consider Figure 14 which shows the influence of external and D:A interfaces.^{11,114–117} In terms of D:A interfaces, thermal annealing led to improved crystallinity (i.e., side chains oriented perpendicular to the substrate) and purity of P3HT donor domains, which improved absorption coefficients and spectral photocurrent of the P3HT:PCBM devices.^{115,116}

Various pre- and post-processing and fabrication strategies change the charge mobilities within the donor and acceptor domains, and therefore the device properties. Of particular interest in this review are morphological design tools that enable improved charge transport in the out-of-plane direction via control of the CP orientation, improvement of domain phase purities, and/or optimization of domain sizes. Much is known about the utilization of such design tools including MW control,¹¹⁸ heteroaromatic ring design,¹¹⁹ copolymer architecture,²³ solvent additives,¹²⁰ copolymer additives, pressure-added solution-based fabrication,^{21,22} off-center spin-



Factors: band alignment, material type, interface morphology

Factors: domain purity, domain size, crystallinity

Figure 14. Role of interfaces in D:A OPV devices. Schematic of a BHJ OPV shown in middle, with relevant layers for operation labelled. The donor and acceptor materials are shown in blue and red, respectively. (middle) Reproduced from ref¹¹ with permission from the American Chemical Society. To the right, the effects of annealing on domain purity, size, and crystallinity a P3HT/PCBM matrix is depicted. (right) Reproduced from ref¹⁴ with permission from John Wiley and sons. The impact of external interfaces is shown to the left of the figure, with factors including band alignment, material type, and interface morphology and schematic showing the band structure of a P3HT/PCBM based device. (left) Reproduced from ref¹⁶ with permission from MDPI.

casting,²⁴ and annealing.^{121,122} Some design strategies, such as the use of molecular dopants,^{123–125} do not have notable effects on the morphology, but significantly improve hole transport because they act as trap-fillers without introducing electronic defects. Continuing to unravel the contributing roles of local composition (i.e., domain purity) and microstructure on the charge transport is important for directed improvements of OPVs comprised of D:A mixtures. To underscore the importance of these contributors, two examples are provided that demonstrate the power of controlling morphology and local composition, and the impact on charge transport and device performance in OPVs. We note that the following examples that we discuss are not intended to be exhaustive. They are chosen because of the in-depth analyses and the employment of unique material systems, including block and gradient copolymers, provide broadly unique insights into the combined roles of local composition and microstructural details that influence charge transport.

5.2 Role of out-of-plane charge transport on OPV performance

The first example highlighting the contributing influences of local composition and structure involves the use of donor copolymers of complex architecture. Amonoo et al. leveraged the copolymer approach to uniquely stabilize the nanoscale

morphology of D:A OPVs.²³ In this case, a gradient copolymer and a block poly(3-hexylselenophene) copolymer with the same constituents, P3HS and P3HT, P(3HS-*g*-3HT) and P(3HS-*b*-3HT), respectively, were implemented as donor materials (the molecules are shown in Figure 15a) with PCBM acceptors. From a light harvesting perspective, the two constituent P3HT and P3HS donor CPs have distinct absorption spectra, and as such, the copolymers of these monomers exhibit broadened absorption profiles. It is evident from Figure 15b, based on energy-filtered transmission electron microscopy (EFTEM) studies, that the morphologies of P3HT:PCBM (see Figure 15b(i)), P3HS:PCBM (see Figure 15b(ii)), P3HS:P3HT(1:1):PCBM (see Figure 15b(iii)), P(3HS-*b*-3HT):PCBM (see Figure 15b(iv)), P(3HS-*g*-3HT):PCBM (see Figure 15b(v)) are each distinct. The dark regions reveal the locations of the polymer-rich regions of the samples. The P(3HS-*g*-3HT):PCBM samples form more uniform and continuous networks of fibrils within the fullerene-rich regions (see Figure 15b(v)), and the P(3HS-*b*-3HT):PCBM samples organize into more dense clusters separate from the fullerene-rich regions owing to the intrinsic self-assembling properties of the block copolymer (see Figure 15b(iv)). Thus, the P(3HS-*g*-3HT):PCBM samples possess larger D:A interfaces with more interconnected pathways for transport due to the unique gradient sequencing of the copolymer as compared to the P(3HS-*b*-3HT):PCBM system.

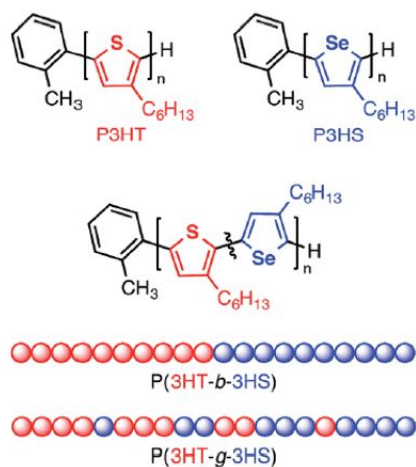
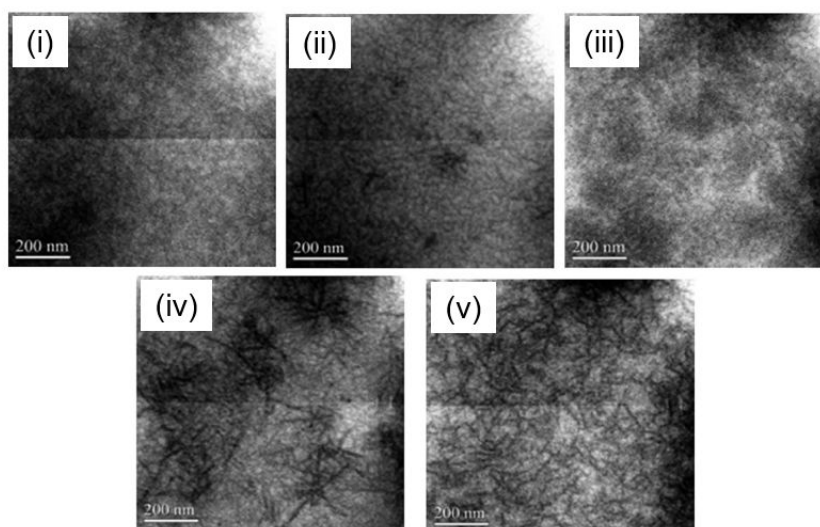
(a) Chemical structures of (co)polymers**(b) EFTEM**

Figure 15. Donor copolymers with complex architecture – structure & composition. (a) Chemical structures of the polymers and copolymers (block – b; gradient – g); (b) Energy- filtered transmission electron microscopy of (i) P3HT:PCBM, (ii) P3HS:PCBM, (iii) P3HS:P3HT(1:1):PCBM, (iv) P(3HS-b-3HT):PCBM, (v) P(3HS-g-3HT):PCBM, with the polymer-rich phase appearing dark. (a) and (b) Reproduced and adapted from ref²³ with permission from the Royal Society of Chemistry.

These D:A morphologies have obvious implications for photo-generated carrier dynamics and charge transport. As measured by photo-CELIV (see Figure 16a), all devices exhibited decreases in carrier density with time, due to carrier recombination. Notably, the gradient donor device had the highest initial carrier density consistent with EFTEM observations of an interconnected network in the active layer, but this device also suffered from high free carrier recombination rates which the authors related to differences in interactions between the copolymer components and PCBM leading to a higher density of trap sites. Local pc-AFM maps (see Figure 16b) revealed that the P(3HS-b-3HT) samples had regions of very low conductivity, attributed to phase-separation of the copolymer or aggregates of PCBM (see Figure 15d(iv)), while the interconnected network of the P(3HS-g-3HT) samples yielded more uniform and higher photocurrent (see Figure 15d(v)) in the out-of-plane direction as compared to other samples. Resultant PCEs from OPV devices that underpinned the findings from photo-CELIV measurements are shown in Figure 16c; in the as-cast devices, despite having high initial carrier density, the P(3HS-g-3HT):PCBM device was outperformed by P3HT:PCBM device due to the high recombination rates. Interestingly, upon thermal stability testing, after 30 minutes the P(3HS-g-3HT):PCBM device had the highest PCE of all devices tested. This result is attributed to the 3HS components mixing with PCBM upon annealing, preventing aggregation of PCBM, and limiting phase separation known to occur in P3HT:PCBM systems. This finding not only demonstrates the utility of the gradient copolymer in both stabilizing the D:A interface during thermal treatment, but also providing microstructure efficient for charge generation and separation. Additionally, this example showcases the role of local structure

in device performance; namely, the creation of continuous and interconnected networks promotes high initial carrier density critical for high-performing OPVs.

The second D:A system example involves the classic 1:1 P3HT:PCBM mixtures undergoing various post-processing treatments. In this work by Green and coworkers, mixtures spin-coated and annealed at 150 °C, considered the "benchmark", were compared to mixtures that underwent super critical carbon dioxide annealing (scCO₂) at 50 °C with varied pressures.¹²² Supercritical (sc) fluid annealing involves tuning of temperature and pressure of materials that are traditionally gasses at standard temperature and pressure (e.g., CO₂) so that the material properties are between a gas and liquid, so-called supercritical fluid. Well known from literature regarding the P3HT:PCBM mixtures are the observations that upon thermal and scCO₂ annealing, the fraction of P3HT amorphous regions decrease from the as-cast case, phase separation between P3HT and PCBM occurs, domains increase in phase purity, and P3HT becomes more crystalline primarily in the alkyl-stacking direction.¹²⁶ EFTEM images showed the phase separation between P3HT and PCBM was greater in thermally annealed and scCO₂ samples than as-cast samples as expected (see Figure 17a). While qualitatively the nanoscale morphologies of the thermally and scCO₂ annealed samples were similar, quantitative extraction of the plasmon peak positions of samples revealed that the scCO₂ samples had the largest mean difference in plasmon peak between the P3HT and PCBM regions, which indicated enhanced purity in these regions (see Figure 17b). Zero-field out-of-plane mobilities extracted via photo-CELIV for similar P3HT:PCBM samples revealed higher mobility values for the thermally annealed mixture ($\mu_{\text{thermal}} = (9.47 \pm 0.96) \times 10^{-2} \text{ cm}^2\text{V}^{-1}\text{s}^{-1}$) as compared to the scCO₂

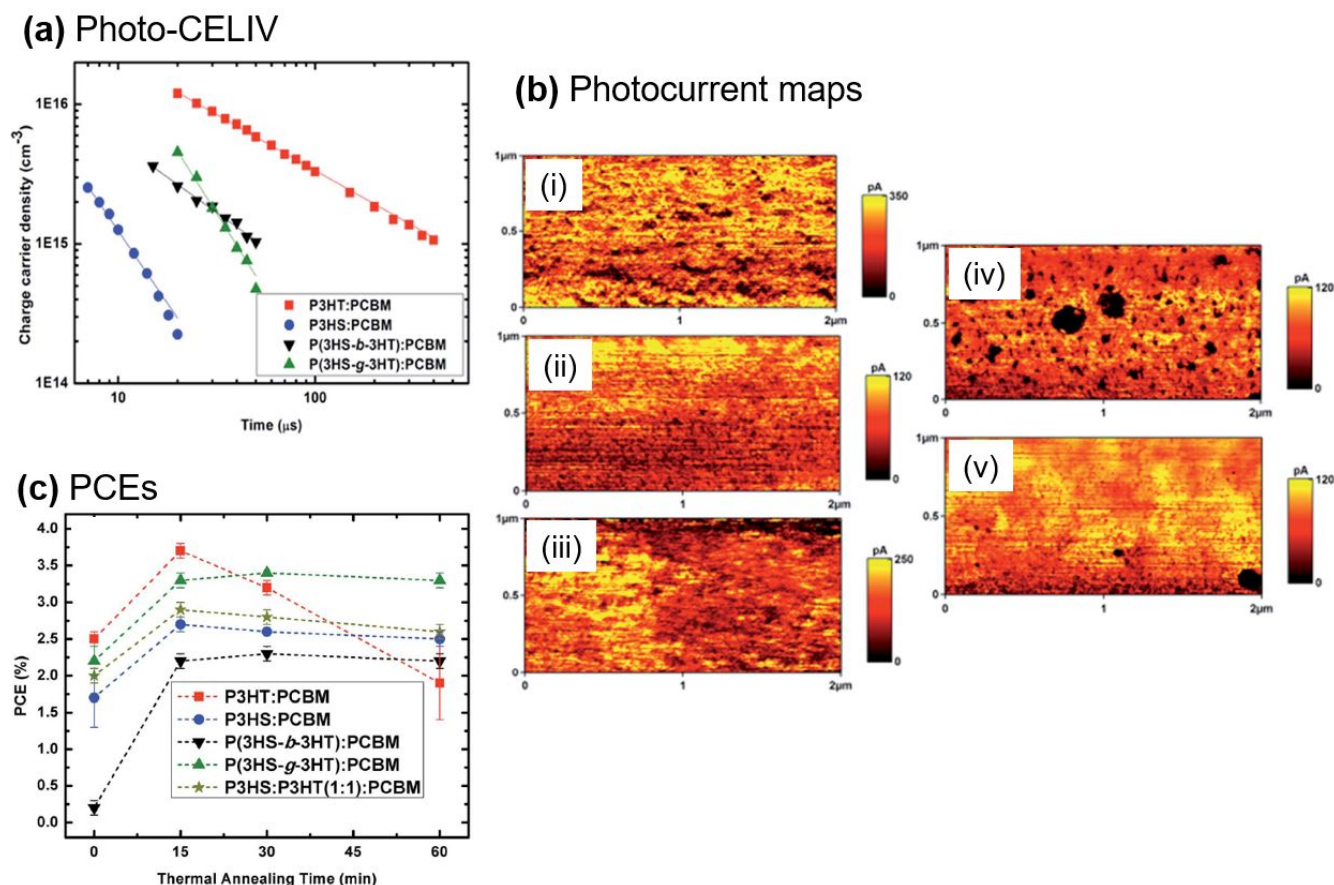


Figure 16. Donor copolymers with complex architecture – charge transport & device performance. (a) Extracted photogenerated charge carriers as a function of delay time measured by photo-CELIV for P3HT:PCBM (red square), P3HS:PCBM (blue circle), P(3HS-*b*-3HT):PCBM (black triangle), P(3HS-*g*-3HT):PCBM (green triangle); (b) Local photocurrent images from pc-AFM of (i) P3HT:PCBM, (ii) P3HS:PCBM, (iii) P3HS:P3HT(1:1):PCBM, (iv) P(3HS-*b*-3HT):PCBM, (v) P(3HS-*g*-3HT):PCBM; (c) PCEs as a function of annealing time for devices from polymer and copolymer blends with PCBM. (a)-(c) Reproduced and adapted from ref²³ with permission from the Royal Society of Chemistry.

annealed mixture ($\mu_{\text{scCO}_2} = (1.59 \pm 0.54) \times 10^{-2} \text{ cm}^2\text{V}^{-1}\text{s}^{-1}$) (see Figure 17c),¹²⁷ though local c-AFM maps showed larger photoconductive areas in the scCO₂ sample as opposed to the thermally-annealed case (see Figure 17d). Overall, PCEs of devices that underwent scCO₂ annealing were higher (2.9%) than either thermally annealed or as-cast P3HT:PCBM-based devices. Obviously, obtaining local structure that improves charge transport is important to device performance, but this example exemplifies the critical nature of domain phase purity, which can be fine tuned along with structure via post-processing routes like scCO₂.

Together, these illustrative examples underscore the key challenges associated with morphological control in two component CP-based systems. Molecular orientation and disorder control of the CP phase are still important for improved charge transport, but the added second phase means the extra considerations of phase purity, composition, domain size and associated D:A area. It should be evident that indeed control of local structure, especially via donor copolymers, leads to increases in initial carrier densities and thermal stability of OPVs. Perhaps of equal or even greater importance, provided

charge mobility is moderately high, is the control of phase purity, as highlighted by the scCO₂ post-processing example. This critical role of domain purity, coupled with domain size, has been demonstrated by others in literature.^{128–130} In a work by Collins et al.,¹²⁹ it was found that the addition of the diiodooctane (DIO) to the casting solution did not significantly change domain composition or crystallinity of the PTB7:PCBM system, but it did lead to decreased domain size and nearly doubled PCEs, suggestive that polymer access to pure fullerene domains is needed for efficient charge separation.¹²⁹ Furthermore, computational work by Lyons, Clarke, and Groves has indicated that sharpening of the interfaces between D:A materials was of significant benefit to device performance.¹³⁰ Obviously, the findings from these examples and literature provide guideposts, but continued study, both with experiment and computation, is needed to promote greater understanding of the interplay between microstructure, domain size, phase purity, and composition in D:A systems and their ultimate impacts on OPV device properties.

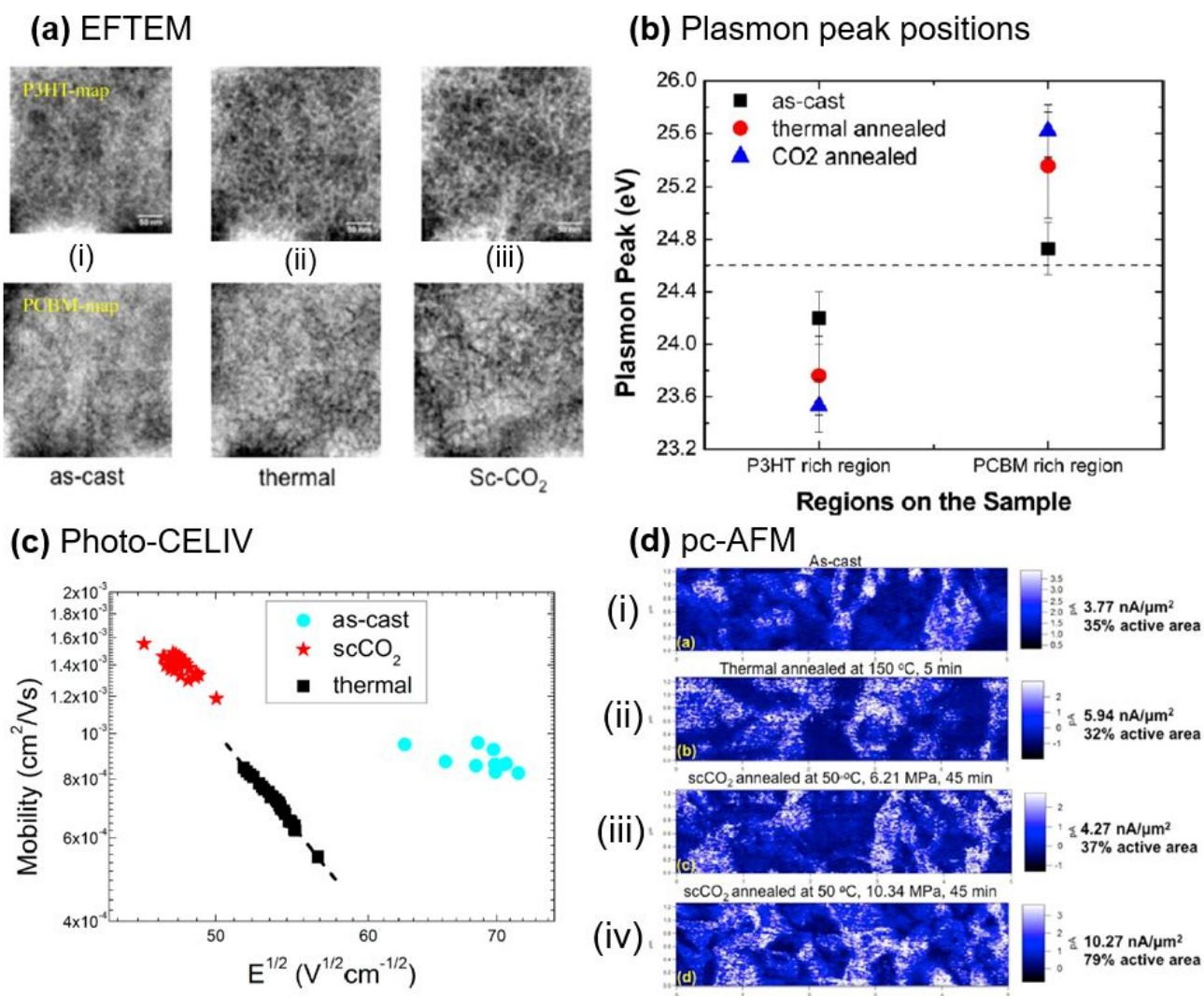


Figure 17. Post-processing of D:A P3HT:PCBM system. 1:1 P3HT:PCBM samples (a) Energy filtered transmission electron microscopy images of (i) as-cast, (ii) thermally annealed at 150 °C, (iii) sc-CO₂ annealed at 50 °C 10.34 MPa for 45 min with P3HT regions appearing bright (top row) and PCBM regions appearing bright (bottom row); (b) plasmon peak positions of P3HT and PCBM rich regions averaged of six EFTEM images for as-cast (black squares), thermally annealed at 150 °C (red circle), and sc-CO₂ annealed at 50 °C 10.34 MPa for 45 min (blue triangle); (c) Electric field dependence of mobility by photo-CELIV of as-cast (blue circles), thermally annealed at 150 °C (black squares), sc-CO₂ annealed (red stars) 50 °C 10.34 MPa. Adapted from ref¹²² (d) Photocurrent maps of (i) as-cast, (ii) thermally annealed at 150 °C, (iii) sc-CO₂ annealed at 50 °C 6.21 MPa for 45 min, (iv) sc-CO₂ annealed at 50 °C 10.34 MPa for 45 min. (a) and (b) and (d) Reproduced and adapted from ref¹²² with permission from the American Chemical Society. (c) Reproduced from ref¹²⁷ with permission from the American Chemical Society.

Conclusions and Outlook

We have reviewed diverse strategies to improve out-of-plane charge transport and subsequent device performance in CP systems, achieved by leveraging a fundamental understanding of charge transport mechanisms and interrelations to morphology. In devices such as diodes and OPVs, such enhancement in out-of-plane mobility promotes improved final device characteristics, though we identify the key combined roles of microstructure, phase purity, and

composition in two component CP systems like OPVs. In single component CP systems, processing methods, chemical modification, thickness confinement, and control of the degree of disorder were discussed as routes to enhance out-of-plane mobility and transport. As mentioned in the Introduction, improving out-of-plane transport in CP systems is very difficult, owing in part to the difficulty of orienting CPs with their fastest transport direction in the vertical direction, so this review is well-positioned to provide targeted approaches to solving this

challenging problem thereby leading to directed advancements in a myriad of optoelectronic devices based on CPs.

Moving forward, further improvements of out-of-plane transport in CPs, via further molecular design strategies and further developments of interrelations between transport mechanisms and morphology, and new experimental methods for better aligning CPs in the vertical direction - maximizing pathways for even higher carrier mobilities. In particular, we recognize the significant promise of controlling the degree of disorder by reducing trap states (section 4.3) and the use of unique processing strategies, like external fields, modified solution-based casting, and vapor-based deposition, as rich future areas of study. Machine learning techniques will, moreover, prove to be essential toward accomplishing these objectives of improved CP alignment and maximized carrier pathways.^{131–133}

Other factors influencing transport should be thoroughly investigated. For example, while modifying electrode chemistry is known to change energy levels, subsequently changing carrier injection/collection energy barriers and OLED and OPV performance, the exact role of electrode chemistries on out-of-plane transport still remains unknown. Local structure and carrier density distribution in the vicinity of polymer/electrode interfaces can significantly influence transport, yet largely remains unexplored in literature. With regards to the latter, as we have alluded to in our review, a majority of studies performed in the past have focused on utilizing processing techniques to study in-plane transport while only limited attention has been paid to transport in the out-of-plane direction. For example, it was recently shown that surface modification coupled with flow-directed self-assembly can yield polymer films with controllable conformation, packing, and chain alignment.¹³⁴ Such progress is expected to bear fruitful results if applied to control and enhance out-of-plane transport. Very recently, Pan et al. demonstrated that exceptional out-of-plane transport in CPs could be achieved by using high magnetic field alignment, a method that has been successfully utilized in the past for aligning liquid crystalline materials.¹³⁵

Finally, moving from electronic transport in single component CP systems to more complex systems, one needs to take into account relevant factors besides charge mobility that impact device performance. We indicated in this review that for OPVs, additional attention must be paid beyond simply improving out-of-plane mobility, as optimized structure for enhanced carrier mobility can have negative impact on carrier generation and recombination, which decreases the PCEs. Similarly, we envision that for other optoelectronic CP-based applications, optimization of transport needs to be considered alongside other factors influencing device figures of merit. For example, in bioelectronic applications that utilize mixed ion-electron conductors, improving out-of-plane electronic transport needs to occur in conjunction with maintaining electron-ion interactions for biosensing.¹³⁶ In skin-electronic, strategies to improve transport need to retain CP mechanical integrity.¹³⁷ Thus, we envision this review to act as a detailed guide toward improvement of out-of-plane charge transport in single component CP systems and as a starting point for more complex CP-based devices in which enhancement of charge transport is highly relevant for directed advancement of next-generation devices.

Author Contributions

JKW, BXD, and PFG wrote and edited the review.

Conflicts of interest

There are no conflicts to declare.

Acknowledgements

Research presented here was enabled in part by support from the Department of Energy, Energy Frontier Research Center, Award No. DE-SC0000957. This work was authored in part by Alliance for Sustainable Energy, LLC, the managed and operator of the National Renewable Energy Laboratory for the U.S. Department of Energy (DOE) under contract No. DE-AC36-08G028308 (PFG). The views expressed in this article do not necessarily represent the views of the DOE or the U.S. Government.

Notes and references

1. Dong, B. X., Wenderott, J. K. & Green, P. F. Charge carrier transport in thin conjugated polymer films: influence of morphology and polymer/substrate interactions. *Colloid Polym. Sci.* (2020). doi:10.1007/s00396-020-04725-1
2. Noriega, R., Rivnay, J., Vandewal, K., Koch, F. P. V., Stingelin, N., Smith, P., Toney, M. F. & Salleo, A. A general relationship between disorder, aggregation and charge transport in conjugated polymers. *Nat. Mater.* **12**, 1038–1044 (2013).
3. Himmelberger, S. & Salleo, A. Engineering semiconducting polymers for efficient charge transport. *MRS Commun.* **5**, 383–395 (2015).
4. Hoffmann, S. T., Bässler, H. & Köhler, A. What Determines Inhomogeneous Broadening of Electronic Transitions in Conjugated Polymers? *J. Phys. Chem. B* **114**, 17037–17048 (2010).
5. Park, K. S., Kwok, J. J., Dilmurat, R., Qu, G., Kafle, P., Luo, X., Jung, S.-H., Olivier, Y., Lee, J.-K., Mei, J., Beljonne, D. & Diao, Y. Tuning conformation, assembly, and charge transport properties of conjugated polymers by printing flow. *Sci. Adv.* **5**, eaaw7757 (2019).
6. Wang, S., Fabiano, S., Himmelberger, S., Puzinas, S., Crispin, X., Salleo, A. & Berggren, M. Experimental evidence that short-range intermolecular aggregation is sufficient for efficient charge transport in conjugated polymers. *Proc. Natl. Acad. Sci.* **112**, 10599–10604 (2015).
7. Fratini, S., Nikolka, M., Salleo, A., Schweicher, G. & Sirringhaus, H. Charge transport in high-mobility conjugated polymers and molecular semiconductors. *Nat. Mater.* **19**, 491–502 (2020).

8. Luo, C., Kyaw, A. K. K., Perez, L. A., Patel, S., Wang, M., Grimm, B., Bazan, G. C., Kramer, E. J. & Heeger, A. J. General Strategy for Self-Assembly of Highly Oriented Nanocrystalline Semiconducting Polymers with High Mobility. *Nano Lett.* **14**, 2764–2771 (2014).
9. Russ, B., Gludell, A., Urban, J. J., Chabinyk, M. L. & Segalman, R. A. Organic thermoelectric materials for energy harvesting and temperature control. *Nat. Rev. Mater.* **1**, 1–14 (2016).
10. Wang, G., Melkonyan, F. S., Facchetti, A. & Marks, T. J. All-Polymer Solar Cells: Recent Progress, Challenges, and Prospects. *Angew. Chem. Int. Ed.* **58**, 4129–4142 (2019).
11. Lu, L., Zheng, T., Wu, Q., Schneider, A. M., Zhao, D. & Yu, L. Recent Advances in Bulk Heterojunction Polymer Solar Cells. *Chem. Rev.* **115**, 12666–12731 (2015).
12. Dang, M. T., Hirsch, L. & Wantz, G. P3HT:PCBM, Best Seller in Polymer Photovoltaic Research. *Adv. Mater.* **23**, 3597–3602 (2011).
13. Yoshikawa, S., Saeki, A., Saito, M., Osaka, I. & Seki, S. On the role of local charge carrier mobility in the charge separation mechanism of organic photovoltaics. *Phys. Chem. Chem. Phys.* **17**, 17778–17784 (2015).
14. Pandey, M., Kumari, N., Nagamatsu, S. & Pandey, S. S. Recent advances in the orientation of conjugated polymers for organic field-effect transistors. *J. Mater. Chem. C* **7**, 13323–13351 (2019).
15. Skrypnichuk, V., Wetzelaer, G.-J. A. H., Gordiichuk, P. I., Mannsfeld, S. C. B., Herrmann, A., Toney, M. F. & Barbero, D. R. Ultrahigh Mobility in an Organic Semiconductor by Vertical Chain Alignment. *Adv. Mater.* **28**, 2359–2366 (2016).
16. Wang, F., Hashimoto, K., Segawa, H. & Tajima, K. Effects of Chain Orientation in Self-Organized Buffer Layers Based on Poly(3-alkylthiophene)s for Organic Photovoltaics. *ACS Appl. Mater. Interfaces* **10**, 8901–8908 (2018).
17. Tsao, H. N. & Müllen, K. Improving polymer transistor performance via morphology control. *Chem. Soc. Rev.* **39**, 2372–2386 (2010).
18. Sirringhaus, H. 25th Anniversary Article: Organic Field-Effect Transistors: The Path Beyond Amorphous Silicon. *Adv. Mater.* **26**, 1319–1335 (2014).
19. Sirringhaus, H. Device Physics of Solution-Processed Organic Field-Effect Transistors. *Adv. Mater.* **17**, 2411–2425 (2005).
20. Salleo, A. Charge transport in polymeric transistors. *Mater. Today* **10**, 38–45 (2007).
21. Park, H. J., Kang, M.-G., Ahn, S. H. & Guo, L. J. A Facile Route to Polymer Solar Cells with Optimum Morphology Readily Applicable to a Roll-to-Roll Process without Sacrificing High Device Performances. *Adv. Mater.* **22**, E247–E253 (2010).
22. Park, H. J., Kim, H., Lee, J. Y., Lee, T. & Guo, L. J. Optimization of polymer photovoltaic cells with bulk heterojunction layers hundreds of nanometers thick: modifying the morphology and cathode interface. *Energy Environ. Sci.* **6**, 2203–2210 (2013).
23. Amonoo, J. A., Li, A., Purdum, G. E., Sykes, M. E., Huang, B., Palermo, E. F., McNeil, A. J., Shtein, M., Loo, Y.-L. & Green, P. F. An all-conjugated gradient copolymer approach for morphological control of polymer solar cells. *J. Mater. Chem. A* **3**, 20174–20184 (2015).
24. Li, A., Bilby, D., Dong, B. X., Amonoo, J., Kim, J. & Green, P. F. Macroscopic alignment of poly(3-hexylthiophene) for enhanced long-range collection of photogenerated carriers. *J. Polym. Sci. Part B Polym. Phys.* **54**, 180–188 (2016).
25. Li, A., Amonoo, J., Huang, B., Goldberg, P. K., McNeil, A. J. & Green, P. F. Enhancing Photovoltaic Performance Using an All-Conjugated Random Copolymer to Tailor Bulk and Interfacial Morphology of the P3HT:ICBA Active Layer. *Adv. Funct. Mater.* **24**, 5594–5602 (2014).
26. Gu, K., Snyder, C. R., Onorato, J., Luscombe, C. K., Bosse, A. W. & Loo, Y.-L. Assessing the Huang–Brown Description of Tie Chains for Charge Transport in Conjugated Polymers. *ACS Macro Lett.* **7**, 1333–1338 (2018).
27. Kline, R. J., McGehee, M. D., Kadnikova, E. N., Liu, J., Fréchet, J. M. J. & Toney, M. F. Dependence of Regioregular Poly(3-hexylthiophene) Film Morphology and Field-Effect Mobility on Molecular Weight. *Macromolecules* **38**, 3312–3319 (2005).
28. Zen, A., Pflaum, J., Hirschmann, S., Zhuang, W., Jaiser, F., Asawapirom, U., Rabe, J. P., Scherf, U. & Neher, D. Effect of Molecular Weight and Annealing of Poly(3-hexylthiophene)s on the Performance of Organic Field-Effect Transistors. *Adv. Funct. Mater.* **14**, 757–764 (2004).

29. Dong, B. X., Smith, M., Strzalka, J., Li, H., McNeil, A. J., Stein, G. E. & Green, P. F. Molecular weight dependent structure and charge transport in MAPLE-deposited poly(3-hexylthiophene) thin films. *J. Polym. Sci. Part B Polym. Phys.* **56**, 652–663 (2018).
30. Koch, F. P. V., Rivnay, J., Foster, S., Müller, C., Downing, J. M., Buchaca-Domingo, E., Westacott, P., Yu, L., Yuan, M., Baklar, M., Fei, Z., Luscombe, C., McLachlan, M. A., Heeney, M., Rumbles, G., Silva, C., Salleo, A., Nelson, J., Smith, P. & Stingelin, N. The impact of molecular weight on microstructure and charge transport in semicrystalline polymer semiconductors—poly(3-hexylthiophene), a model study. *Prog. Polym. Sci.* **38**, 1978–1989 (2013).
31. Gasperini, A. & Sivula, K. Effects of Molecular Weight on Microstructure and Carrier Transport in a Semicrystalline Poly(thieno)thiophene. *Macromolecules* **46**, 9349–9358 (2013).
32. Schwarze, M., Gaul, C., Scholz, R., Bussolotti, F., Hofacker, A., Schellhammer, K. S., Nell, B., Naab, B. D., Bao, Z., Spoltore, D., Vandewal, K., Widmer, J., Kera, S., Ueno, N., Ortmann, F. & Leo, K. Molecular parameters responsible for thermally activated transport in doped organic semiconductors. *Nat. Mater.* **18**, 242–248 (2019).
33. Zhang, X., Bronstein, H., Kronemeijer, A. J., Smith, J., Kim, Y., Kline, R. J., Richter, L. J., Anthopoulos, T. D., Sirringhaus, H., Song, K., Heeney, M., Zhang, W., McCulloch, I. & DeLongchamp, D. M. Molecular origin of high field-effect mobility in an indacenodithiophene–benzothiadiazole copolymer. *Nat. Commun.* **4**, 2238 (2013).
34. Li, Y., Tatum, W. K., Onorato, J. W., Zhang, Y. & Luscombe, C. K. Low Elastic Modulus and High Charge Mobility of Low-Crystallinity Indacenodithiophene-Based Semiconducting Polymers for Potential Applications in Stretchable Electronics. *Macromolecules* **51**, 6352–6358 (2018).
35. Venkateshvaran, D., Nikolka, M., Sadhanala, A., Lemaire, V., Zelazny, M., Kepa, M., Hurhangee, M., Kronemeijer, A. J., Pecunia, V., Nasrallah, I., Romanov, I., Broch, K., McCulloch, I., Emin, D., Olivier, Y., Cornil, J., Beljonne, D. & Sirringhaus, H. Approaching disorder-free transport in high-mobility conjugated polymers. *Nature* **515**, 384–388 (2014).
36. Zhao, Y., Guo, Y. & Liu, Y. 25th Anniversary Article: Recent Advances in n-Type and Ambipolar Organic Field-Effect Transistors. *Adv. Mater.* **25**, 5372–5391 (2013).
37. Nielsen, C. B., Turbiez, M. & McCulloch, I. Recent Advances in the Development of Semiconducting DPP-Containing Polymers for Transistor Applications. *Adv. Mater.* **25**, 1859–1880 (2013).
38. Haneef, H. F., Zeidell, A. M. & Jurchescu, O. D. Charge carrier traps in organic semiconductors: a review on the underlying physics and impact on electronic devices. *J. Mater. Chem. C* **8**, 759–787 (2020).
39. Horowitz, G. & Delannoy, P. An analytical model for organic-based thin-film transistors. *J. Appl. Phys.* **70**, 469 (1998).
40. Chua, L.-L., Ho, P. K. H., Sirringhaus, H. & Friend, R. H. Observation of Field-Effect Transistor Behavior at Self-Organized Interfaces. *Adv. Mater.* **16**, 1609–1615 (2004).
41. Chua, L.-L., Zaumseil, J., Chang, J.-F., Ou, E. C.-W., Ho, P. K.-H., Sirringhaus, H. & Friend, R. H. General observation of n-type field-effect behaviour in organic semiconductors. *Nature* **434**, 194–199 (2005).
42. Tanase, C., Meijer, E. J., Blom, P. W. M. & de Leeuw, D. M. Unification of the Hole Transport in Polymeric Field-Effect Transistors and Light-Emitting Diodes. *Phys. Rev. Lett.* **91**, 216601 (2003).
43. Li, A., Dong, B. X. & Green, P. F. Influence of morphological disorder on in- and out-of-plane charge transport in conjugated polymer films. *MRS Commun.* **5**, 593–598 (2015).
44. Dong, B. X., Li, A., Strzalka, J., Stein, G. E. & Green, P. F. Molecular organization in MAPLE-deposited conjugated polymer thin films and the implications for carrier transport characteristics. *J. Polym. Sci. Part B Polym. Phys.* **55**, 39–48 (2017).
45. Juška, G., Arlauskas, K., Viliūnas, M. & Kočka, J. Extraction Current Transients: New Method of Study of Charge Transport in Microcrystalline Silicon. *Phys. Rev. Lett.* **84**, 4946–4949 (2000).
46. Bäessler, H. Charge Transport in Disordered Organic Photoconductors a Monte Carlo Simulation Study. *Phys. Status Solidi B* **175**, 15–56 (1993).
47. Goh, C., Kline, R. J., McGehee, M. D., Kadnikova, E. N. & Fréchet, J. M. J. Molecular-weight-dependent mobilities in regioregular poly(3-hexylthiophene) diodes. *Appl. Phys. Lett.* **86**, 122110 (2005).

48. Sirringhaus, H., Bird, M. & Zhao, N. Charge Transport Physics of Conjugated Polymer Field-Effect Transistors. *Adv. Mater.* **22**, 3893–3898 (2010).
49. Spear, W. E. Drift mobility techniques for the study of electrical transport properties in insulating solids. *J. Non-Cryst. Solids* **1**, 197–214 (1969).
50. Gambino, S., Bansal, A. K. & Samuel, I. D. W. Comparison of hole mobility in thick and thin films of a conjugated polymer. *Org. Electron.* **11**, 467–471 (2010).
51. Kim, J. Y., Cho, H., Noh, S., Lee, Y., Nam, Y. M., Lee, C. & Jo, W. H. Charge transport in amorphous low bandgap conjugated polymer/fullerene films. *J. Appl. Phys.* **111**, 043710 (2012).
52. Shimata, Y. & Saeki, A. Hole Relaxation in Polymer:Fullerene Solar Cells Examined by the Simultaneous Measurement of Time-of-Flight and Time-Resolved Microwave Conductivity. *J. Phys. Chem. C* **121**, 18351–18359 (2017).
53. Facchetti, A. Polymer donor–polymer acceptor (all-polymer) solar cells. *Mater. Today* **16**, 123–132 (2013).
54. Kokil, A., Yang, K. & Kumar, J. Techniques for characterization of charge carrier mobility in organic semiconductors. *J. Polym. Sci. Part B Polym. Phys.* **50**, 1130–1144 (2012).
55. Juška, G., Nekrašas, N. & Genevičius, K. Investigation of charge carriers transport from extraction current transients of injected charge carriers. *J. Non-Cryst. Solids* **358**, 748–750 (2012).
56. Pivrikas, a., Juška, G., Österbacka, R., Westerling, M., Viliūnas, M., Arlauskas, K. & Stubb, H. Langevin recombination and space-charge-perturbed current transients in regiorandom poly(3-hexylthiophene). *Phys. Rev. B* **71**, 125205 (2005).
57. Juska, G., Arlauskas, K., Viliunas, M. & Kocka, J. Extraction current transients: new method of study of charge transport in microcrystalline silicon. *Phys. Rev. Lett.* **84**, 4946–9 (2000).
58. Juška, G., Arlauskas, K., Viliūnas, M., Genevičius, K., Österbacka, R. & Stubb, H. Charge transport in π -conjugated polymers from extraction current transients. *Phys. Rev. B* **62**, R16235–R16238 (2000).
59. Pivrikas, A., Sariciftci, N. S., Juška, G. & Österbacka, R. A review of charge transport and recombination in polymer/fullerene organic solar cells. *Prog. Photovolt. Res. Appl.* **15**, 677–696 (2007).
60. Dong, B. X., Huang, B., Tan, A. & Green, P. F. Nanoscale Orientation Effects on Carrier Transport in a Low-Band-Gap Polymer. *J. Phys. Chem. C* **118**, 17490–17498 (2014).
61. Huang, B., Glynos, E., Frieberg, B., Yang, H. & Green, P. F. Effect of Thickness-Dependent Structural Evolution on Out-of-plane Hole Mobility in Poly(3-hexylthiophene) Films. *ACS Appl. Mater. Interfaces* (2012). doi:10.1021/am3011252
62. Juška, G., Nekrašas, N., Valentinavičius, V., Meredith, P. & Pivrikas, A. Extraction of photogenerated charge carriers by linearly increasing voltage in the case of Langevin recombination. *Phys. Rev. B* **84**, 155202 (2011).
63. Mott, N. F. & Gurney, R. W. Electronic processes in ionic crystals. (1964).
64. Dacuña, J. & Salleo, a. Modeling Space-Charge Limited Currents in Organic Semiconductors : Extracting Trap Density and Mobility I . Introduction. *Phys. Rev. B* **84**, 195209 (2011).
65. Campbell, A. J., Bradley, D. D. C. & Lidzey, D. G. Space-charge limited conduction with traps in poly(phenylene vinylene) light emitting diodes. *J. Appl. Phys.* **82**, 6326–6342 (1997).
66. Blom, P. W. M., de Jong, M. J. M. & Vleggaar, J. J. M. Electron and hole transport in poly(p-phenylene vinylene) devices. *Appl. Phys. Lett.* **68**, 3308–3310 (1996).
67. Jurchescu, O. D., Baas, J. & Palstra, T. T. M. Effect of impurities on the mobility of single crystal pentacene. *Appl. Phys. Lett.* **84**, 3061–3063 (2004).
68. Goetz, K. P. & Jurchescu, O. D. *Conductivity measurements of organic materials using field-effect transistors (FETs) and space-charge-limited current (SCLC) techniques. Handb. Org. Mater. Electron. Photonic Devices* (Elsevier Ltd., 2019). doi:10.1016/b978-0-08-102284-9.00014-0
69. Alexeev, A., Loos, J. & Koetse, M. M. Nanoscale electrical characterization of semiconducting polymer blends by conductive atomic force microscopy (C-AFM). *Ultramicroscopy* **106**, 191–199 (2006).
70. Alekseev, A., Yedrissov, A., Hedley, G. J., Ibraikulov, O., Heiser, T., Samuel, I. D. W. & Kharintsev, S. Nanoscale mobility mapping in semiconducting polymer films. *Ultramicroscopy* **218**, 113081 (2020).

71. Moerman, D., Sebaihi, N., Kaviyil, S. E., Leclère, P., Lazzaroni, R. & Douhéret, O. Towards a unified description of the charge transport mechanisms in conductive atomic force microscopy studies of semiconducting polymers. *Nanoscale* **6**, 10596–10603 (2014).
72. Coffey, D. C., Reid, O. G., Rodovsky, D. B., Bartholomew, G. P. & Ginger, D. S. Mapping Local Photocurrents in Polymer/Fullerene Solar Cells with Photoconductive Atomic Force Microscopy. *Nano Lett.* **7**, 738–744 (2007).
73. Caballero-Quintana, I., Maldonado, J.-L., Meneses-Nava, M.-A., Barbosa-García, O., Valenzuela-Benavides, J. & Bousseksou, A. Semiconducting Polymer Thin Films Used in Organic Solar Cells: A Scanning Tunneling Microscopy Study. *Adv. Electron. Mater.* **5**, 1800499 (2019).
74. Wenderott, J. K., Raghav, A., Shtein, M., Green, P. F. & Satapathi, S. Local Optoelectronic Characterization of Solvent-Annealed, Lead-Free, Bismuth-Based Perovskite Films. *Langmuir* **34**, 7647–7654 (2018).
75. Reid, O. G., Munechika, K. & Ginger, D. S. Space Charge Limited Current Measurements on Conjugated Polymer Films using Conductive Atomic Force Microscopy. *Nano Lett.* **8**, 1602–1609 (2008).
76. Sirringhaus, H., Brown, P. J., Friend, R. H., Nielsen, M. M., Bechgaard, K., Langeveld-Voss, B. M. W., Spiering, A. J. H., Janssen, R. a. J., Meijer, E. W., Herwig, P. & de Leeuw, D. M. Two-dimensional charge transport in self-organized, high-mobility conjugated polymers. *Nature* **401**, 685–688 (1999).
77. Dong, B. X., Amonoo, J. A., Purdum, G. E., Loo, Y.-L. & Green, P. F. Enhancing Carrier Mobilities in Organic Thin-Film Transistors Through Morphological Changes at the Semiconductor/Dielectric Interface Using Supercritical Carbon Dioxide Processing. *ACS Appl. Mater. Interfaces* **8**, 31144–31153 (2016).
78. McCulloch, I., Heeney, M., Bailey, C., Genevicius, K., MacDonald, I., Shkunov, M., Sparrowe, D., Tierney, S., Wagner, R., Zhang, W., Chabinyc, M. L., Kline, R. J., McGehee, M. D. & Toney, M. F. Liquid-crystalline semiconducting polymers with high charge-carrier mobility. *Nat. Mater.* **5**, 328–333 (2006).
79. DeLongchamp, D. M., Kline, R. J., Lin, E. K., Fischer, D. A., Richter, L. J., Lucas, L. A., Heeney, M., McCulloch, I. & Northrup, J. E. High Carrier Mobility Polythiophene Thin Films: Structure Determination by Experiment and Theory. *Adv. Mater.* **19**, 833–837 (2007).
80. Zhang, X., Richter, L. J., DeLongchamp, D. M., Kline, R. J., Hammond, M. R., McCulloch, I., Heeney, M., Ashraf, R. S., Smith, J. N., Anthopoulos, T. D., Schroeder, B., Geerts, Y. H., Fischer, D. A. & Toney, M. F. Molecular Packing of High-Mobility Diketo Pyrrolo-Pyrrole Polymer Semiconductors with Branched Alkyl Side Chains. *J. Am. Chem. Soc.* **133**, 15073–15084 (2011).
81. Yuan, Y., Giri, G., Ayzner, A. L., Zoombelt, A. P., Mannsfeld, S. C. B., Chen, J., Nordlund, D., Toney, M. F., Huang, J. & Bao, Z. Ultra-high mobility transparent organic thin film transistors grown by an off-centre spin-coating method. *Nat. Commun.* **5**, 3005 (2014).
82. Jimison, L. H., Toney, M. F., McCulloch, I., Heeney, M. & Salleo, A. Charge-Transport Anisotropy Due to Grain Boundaries in Directionally Crystallized Thin Films of Regioregular Poly(3-hexylthiophene). *Adv. Mater.* **21**, 1568–1572 (2009).
83. Brinkmann, M. & Rannou, P. Effect of Molecular Weight on the Structure and Morphology of Oriented Thin Films of Regioregular Poly(3-hexylthiophene) Grown by Directional Epitaxial Solidification. *Adv. Funct. Mater.* **17**, 101–108 (2007).
84. Hamidi-Sakr, A., Biniek, L., Bantignies, J.-L., Maurin, D., Herrmann, L., Leclerc, N., Lévêque, P., Vijayakumar, V., Zimmermann, N. & Brinkmann, M. A Versatile Method to Fabricate Highly In-Plane Aligned Conducting Polymer Films with Anisotropic Charge Transport and Thermoelectric Properties: The Key Role of Alkyl Side Chain Layers on the Doping Mechanism. *Adv. Funct. Mater.* n/a-n/a (2017). doi:10.1002/adfm.201700173
85. Xu, G., Bao, Z. & Groves, J. T. Langmuir–Blodgett Films of Regioregular Poly(3-hexylthiophene) as Field-Effect Transistors. *Langmuir* **16**, 1834–1841 (2000).
86. Aryal, M., Trivedi, K. & Hu, W. (Walter). Nano-Confinement Induced Chain Alignment in Ordered P3HT Nanostructures Defined by Nanoimprint Lithography. *ACS Nano* **3**, 3085–3090 (2009).
87. O'Connor, B., Kline, R. J., Conrad, B. R., Richter, L. J., Gundlach, D., Toney, M. F. & DeLongchamp, D. M. Anisotropic Structure and Charge Transport in

- Highly Strain-Aligned Regioregular Poly(3-hexylthiophene). *Adv. Funct. Mater.* **21**, 3697–3705 (2011).
88. Gargi, D., Kline, R. J., DeLongchamp, D. M., Fischer, D. A., Toney, M. F. & O'Connor, B. T. Charge Transport in Highly Face-On Poly(3-hexylthiophene) Films. *J. Phys. Chem. C* **117**, 17421–17428 (2013).
89. Ye, Z., Yang, X., Cui, H. & Qiu, F. Nanowires with unusual packing of poly(3-hexylthiophene)s induced by electric fields. *J. Mater. Chem. C* **2**, 6773–6780 (2014).
90. Diao, Y., Shaw, L., Bao, Z. & Mannsfeld, S. C. B. Morphology control strategies for solution-processed organic semiconductor thin films. *Energy Environ. Sci.* **7**, 2145–2159 (2014).
91. Tseng, H.-R., Phan, H., Luo, C., Wang, M., Perez, L. A., Patel, S. N., Ying, L., Kramer, E. J., Nguyen, T.-Q., Bazan, G. C. & Heeger, A. J. High-Mobility Field-Effect Transistors Fabricated with Macroscopic Aligned Semiconducting Polymers. *Adv. Mater.* **26**, 2993–2998 (2014).
92. Duong, D. T., Toney, M. F. & Salleo, A. Role of confinement and aggregation in charge transport in semicrystalline polythiophene thin films. *Phys. Rev. B* **86**, 205205 (2012).
93. Kajiya, D., Ozawa, S., Koganezawa, T. & Saitow, K. Enhancement of Out-of-plane Mobility in P3HT Film by Rubbing: Aggregation and Planarity Enhanced with Low Regioregularity. *J. Phys. Chem. C* **119**, 7987–7995 (2015).
94. Kajiya, D., Koganezawa, T. & Saitow, K. Enhancement of Out-of-Plane Mobilities of Three Poly(3-alkylthiophene)s and Associated Mechanism. *J. Phys. Chem. C* **120**, 23351–23357 (2016).
95. Liang, Y., Feng, D., Wu, Y., Tsai, S.-T., Li, G., Ray, C. & Yu, L. Highly Efficient Solar Cell Polymers Developed via Fine-Tuning of Structural and Electronic Properties. *J. Am. Chem. Soc.* **131**, 7792–7799 (2009).
96. Liang, Y., Xu, Z., Xia, J., Tsai, S.-T., Wu, Y., Li, G., Ray, C. & Yu, L. For the Bright Future—Bulk Heterojunction Polymer Solar Cells with Power Conversion Efficiency of 7.4%. *Adv. Mater.* **22**, E135–E138 (2010).
97. Ma, J., Hashimoto, K., Koganezawa, T. & Tajima, K. End-On Orientation of Semiconducting Polymers in Thin Films Induced by Surface Segregation of Fluoroalkyl Chains. *J. Am. Chem. Soc.* **135**, 9644–9647 (2013).
98. Steyrlleuthner, R., Schubert, M., Jaiser, F., Blakesley, J. C., Chen, Z., Facchetti, A. & Neher, D. Bulk Electron Transport and Charge Injection in a High Mobility n-Type Semiconducting Polymer. *Adv. Mater.* **22**, 2799–2803 (2010).
99. Yang, H., Glynos, E., Huang, B. & Green, P. F. Out-of-Plane Carrier Transport in Conjugated Polymer Thin Films: Role of Morphology. *J. Phys. Chem. C* **117**, 9590–9597 (2013).
100. Nikolka, M., Broch, K., Armitage, J., Hanifi, D., Nowack, P. J., Venkateshvaran, D., Sadhanala, A., Saska, J., Mascal, M., Jung, S.-H., Lee, J.-K., McCulloch, I., Salleo, A. & Sirringhaus, H. High-mobility, trap-free charge transport in conjugated polymer diodes. *Nat. Commun.* **10**, 2122 (2019).
101. Chen, W., Xu, T., He, F., Wang, W., Wang, C., Strzalka, J., Liu, Y., Wen, J., Miller, D. J., Chen, J., Hong, K., Yu, L. & Darling, S. B. Hierarchical Nanomorphologies Promote Exciton Dissociation in Polymer/Fullerene Bulk Heterojunction Solar Cells. *Nano Lett.* **11**, 3707–3713 (2011).
102. Carsten, B., Szarko, J. M., Son, H. J., Wang, W., Lu, L., He, F., Rolczynski, B. S., Lou, S. J., Chen, L. X. & Yu, L. Examining the Effect of the Dipole Moment on Charge Separation in Donor–Acceptor Polymers for Organic Photovoltaic Applications. *J. Am. Chem. Soc.* **133**, 20468–20475 (2011).
103. Lu, L. & Yu, L. Understanding Low Bandgap Polymer PTB7 and Optimizing Polymer Solar Cells Based on It. *Adv. Mater.* **26**, 4413–4430 (2014).
104. Guo, J., Liang, Y., Szarko, J., Lee, B., Son, H. J., Rolczynski, B. S., Yu, L. & Chen, L. X. Structure, Dynamics, and Power Conversion Efficiency Correlations in a New Low Bandgap Polymer: PCBM Solar Cell. *J. Phys. Chem. B* **114**, 742–748 (2010).
105. Steyrlleuthner, R., Di Pietro, R., Collins, B. A., Polzer, F., Himmelberger, S., Schubert, M., Chen, Z., Zhang, S., Salleo, A., Ade, H., Facchetti, A. & Neher, D. The Role of Regioregularity, Crystallinity, and Chain Orientation on Electron Transport in a High-Mobility n-Type Copolymer. *J. Am. Chem. Soc.* **136**, 4245–4256 (2014).
106. Rivnay, J., Toney, M. F., Zheng, Y., Kauvar, I. V., Chen, Z., Wagner, V., Facchetti, A. & Salleo, A. Unconventional Face-On Texture and Exceptional In-Plane Order of a High Mobility n-Type Polymer. *Adv. Mater.* **22**, 4359–4363 (2010).
107. Green, P. F. Wetting and dynamics of structured liquid films. *J. Polym. Sci. Part B Polym. Phys.* **41**, 2219–2235 (2003).

108. Coulon, G., Russell, T. P., Deline, V. R. & Green, P. F. Surface-induced orientation of symmetric, diblock copolymers: a secondary ion mass-spectrometry study. *Macromolecules* **22**, 2581–2589 (1989).
109. Jimison, L. H., Himmelberger, S., Duong, D. T., Rivnay, J., Toney, M. F. & Salleo, A. Vertical confinement and interface effects on the microstructure and charge transport of P3HT thin films. *J. Polym. Sci. Part B Polym. Phys.* **51**, 611–620 (2013).
110. Cheon, K. H., Cho, J., Lim, B. T., Yun, H.-J., Kwon, S.-K., Kim, Y.-H. & Chung, D. S. Analysis of charge transport in high-mobility diketopyrrolopyrrole polymers by space charge limited current and time of flight methods. *RSC Adv.* **4**, 35344–35347 (2014).
111. Schott, S., Gann, E., Thomsen, L., Jung, S.-H., Lee, J.-K., McNeill, C. R. & Sirringhaus, H. Charge-Transport Anisotropy in a Uniaxially Aligned Diketopyrrolopyrrole-Based Copolymer. *Adv. Mater.* **27**, 7356–7364 (2015).
112. Ma, W., Tumbleston, J. R., Wang, M., Gann, E., Huang, F. & Ade, H. Domain Purity, Miscibility, and Molecular Orientation at Donor/Acceptor Interfaces in High Performance Organic Solar Cells: Paths to Further Improvement. *Adv. Energy Mater.* **3**, 864–872 (2013).
113. Yu, G., Gao, J., Hummelen, J. C., Wudl, F. & Heeger, A. J. Polymer Photovoltaic Cells: Enhanced Efficiencies via a Network of Internal Donor-Acceptor Heterojunctions. *Science* **270**, 1789–1791 (1995).
114. Erb, T., Zhokhavets, U., Gobsch, G., Raleva, S., Stühn, B., Schilinsky, P., Waldauf, C. & Brabec, C. J. Correlation Between Structural and Optical Properties of Composite Polymer/Fullerene Films for Organic Solar Cells. *Adv. Funct. Mater.* **15**, 1193–1196 (2005).
115. Walker, B., Choi, H. & Kim, J. Y. Interfacial engineering for highly efficient organic solar cells. *Curr. Appl. Phys.* **17**, 370–391 (2017).
116. Zeng, H., Zhu, X., Liang, Y. & Guo, X. Interfacial Layer Engineering for Performance Enhancement in Polymer Solar Cells. *Polymers* **7**, 333–372 (2015).
117. Guo, X., Zhou, N., Lou, S. J., Smith, J., Tice, D. B., Hennek, J. W., Ortiz, R. P., Navarrete, J. T. L., Li, S., Strzalka, J., Chen, L. X., Chang, R. P. H., Facchetti, A. & Marks, T. J. Polymer solar cells with enhanced fill factors. *Nat. Photonics* **7**, 825–833 (2013).
118. Park, J. B., Ha, J.-W., Jung, I. H. & Hwang, D.-H. High-Performance Nonfullerene Organic Photovoltaic Cells Using a TPD-Based Wide Bandgap Donor Polymer. *ACS Appl. Energy Mater.* **2**, 5692–5697 (2019).
119. Kim, J.-H., Shin, S. A., Park, J. B., Song, C. E., Shin, W. S., Yang, H., Li, Y. & Hwang, D.-H. Fluorinated Benzoselenadiazole-Based Low-Band-Gap Polymers for High Efficiency Inverted Single and Tandem Organic Photovoltaic Cells. *Macromolecules* **47**, 1613–1622 (2014).
120. Ho, C. H. Y., Dong, Q., Yin, H., Leung, W. W. K., Yang, Q., Lee, H. K. H., Tsang, S. W. & So, S. K. Impact of Solvent Additive on Carrier Transport in Polymer:Fullerene Bulk Heterojunction Photovoltaic Cells. *Adv. Mater. Interfaces* **2**, 1500166 (2015).
121. Jagadamma, L. K., Sajjad, M. T., Savikhin, V., Toney, M. F. & Samuel, I. D. W. Correlating photovoltaic properties of a PTB7-Th:PC71BM blend to photophysics and microstructure as a function of thermal annealing. *J. Mater. Chem. A* **5**, 14646–14657 (2017).
122. Amonoo, J. A., Glynos, E., Chen, X. C. & Green, P. F. An Alternative Processing Strategy for Organic Photovoltaic Devices Using a Supercritical Fluid. *J. Phys. Chem. C* **116**, 20708–20716 (2012).
123. Yan, H., Manion, J. G., Yuan, M., Arquer, F. P. G. de, McKeown, G. R., Beaupré, S., Leclerc, M., Sargent, E. H. & Seferos, D. S. Increasing Polymer Solar Cell Fill Factor by Trap-Filling with F4-TCNQ at Parts Per Thousand Concentration. *Adv. Mater.* **28**, 6491–6496 (2016).
124. Loiudice, A., Rizzo, A., Biasiucci, M. & Gigli, G. Bulk Heterojunction versus Diffused Bilayer: The Role of Device Geometry in Solution p-Doped Polymer-Based Solar Cells. *J. Phys. Chem. Lett.* **3**, 1908–1915 (2012).
125. Hou, T., Liu, F., Wang, Z., Zhang, Y., Wei, Q., Li, B., Zhang, S. & Xing, G. Trap-Filling-Induced Charge Carrier Dynamics in Organic Solar Cells. *Adv. Opt. Mater.* **6**, 1800027 (2018).
126. Treat, N. D., Brady, M. A., Smith, G., Toney, M. F., Kramer, E. J., Hawker, C. J. & Chabiniy, M. L. Interdiffusion of PCBM and P3HT Reveals Miscibility in a Photovoltaically Active Blend. *Adv. Energy Mater.* **1**, 82–89 (2011).
127. Huang, B., Amonoo, J. A., Li, A., Chen, X. C. & Green, P. F. Role of Domain Size and Phase Purity

- on Charge Carrier Density, Mobility, and Recombination in Poly(3-hexylthiophene):Phenyl-C61-butyric Acid Methyl Ester Devices. *J. Phys. Chem. C* **118**, 3968–3975 (2014).
128. Zhang, Q., Chen, Z., Ma, W., Xie, Z. & Han, Y. Optimizing domain size and phase purity in all-polymer solar cells by solution ordered aggregation and confinement effect of the acceptor. *J. Mater. Chem. C* **7**, 12560–12571 (2019).
129. Collins, B. A., Li, Z., Tumbleston, J. R., Gann, E., McNeill, C. R. & Ade, H. Absolute Measurement of Domain Composition and Nanoscale Size Distribution Explains Performance in PTB7:PC71BM Solar Cells. *Adv. Energy Mater.* **3**, 65–74 (2013).
130. Lyons, B. P., Clarke, N. & Groves, C. The relative importance of domain size, domain purity and domain interfaces to the performance of bulk-heterojunction organic photovoltaics. *Energy Environ. Sci.* **5**, 7657–7663 (2012).
131. Saeki, A. & Kranthiraja, K. A high throughput molecular screening for organic electronics via machine learning: present status and perspective. *Jpn. J. Appl. Phys.* **59**, SD0801 (2019).
132. Sahu, H., Rao, W., Troisi, A. & Ma, H. Toward Predicting Efficiency of Organic Solar Cells via Machine Learning and Improved Descriptors. *Adv. Energy Mater.* **8**, 1801032 (2018).
133. Kranthiraja, K. & Saeki, A. Experiment-Oriented Machine Learning of Polymer:Non-Fullerene Organic Solar Cells. *Adv. Funct. Mater.* **n/a**, 2011168
134. Park, K. S., Kwok, J. J., Kafle, P. & Diao, Y. When Assembly Meets Processing: Tuning Multiscale Morphology of Printed Conjugated Polymers for Controlled Charge Transport. *Chem. Mater.* **33**, 469–498 (2021).
135. Pan, G., Hu, L., Zhang, F. & Chen, Q. Out-of-Plane Alignment of Conjugated Semiconducting Polymers by Horizontal Rotation in a High Magnetic Field. *J. Phys. Chem. Lett.* **12**, 3476–3484 (2021).
136. Paulsen, B. D., Tybrandt, K., Stavrinidou, E. & Rivnay, J. Organic mixed ionic–electronic conductors. *Nat. Mater.* **19**, 13–26 (2020).
137. Tran, H., Feig, V. R., Liu, K., Zheng, Y. & Bao, Z. Polymer Chemistries Underpinning Materials for Skin-Inspired Electronics. *Macromolecules* **52**, 3965–3974 (2019).